Mechanical Stresses in Vocal Fold Tissue during Voice Production

A thesis presented by

Heather Elspeth Gunter

to

The Division of Engineering & Applied Sciences

in partial fulfillment of the requirements

for the degree of

Doctor of Philosophy

in the subject of

Engineering Sciences

Harvard University

Cambridge, Massachusetts

May, 2003

ABSTRACT

Mechanical Stresses in Vocal Fold Tissue During Voice Production

Advisor: Robert D. Howe **Author: Heather Elspeth Gunter**

Theoretical and experimental techniques are used to study the tissue mechanics governing vocal fold closure and collision during phonation in order to evaluate the development of stresses that may be risk factors for pathology development. An original three-dimensional finite element model of vocal fold tissue predicts these quantities with high spatial resolution. Models predict that compressive stress in three directions and vertical shear stress are increased during collision in the typical location of lesions (i.e. the center of the superior medial edge of the vocal fold in the middle of the vibrating and contact region). This supports the hypothesis that stress is a cause of vocal fold pathology, and suggests modes of tissue injury. Predictions of increased stress due to increased voicing intensity are consistent with the hypothesis and clinical observations that loud voicing is a risk factor for benign vocal fold pathology development. Additional finite element models include a representation of the superficial lamina propria (SLP), which is a soft tissue layer near the surface of the vocal folds that

contributes to voice quality and vocal fold injury. Increases in SLP stiffness are associated with increases in compressive and shear stresses in both the epithelium and SLP during collision. Increases in SLP stiffness are also associated with decreases in longitudinal tensile stress in the epithelium prior to collision. These results support the proposed role of SLP stiffness in determining mechanical stress and injury risk, and guide design and selection of SLP replacements used in vocal fold augmentation surgery. In vivo vocal fold collision forces in humans are measured using a new low profile force sensor that minimizes measurement artifacts and maintains voice quality. Impact force correlates more strongly with voice intensity than pitch. The finite element models translate increased force magnitudes into increases in compressive stress, vertical shear stress and Von Mises stress magnitudes. Avoidance of the conditions of increased collision force may prevent development of lesions.

TABLE OF CONTENTS

Abstract iii

Table of contents v

List of figures and tables viii

Acknowledgements xii

Chapter 1: Introduction 1

Mechanics of vocal fold tissue 6

Research objectives and thesis organization 9

Chapter 2: A mechanical model of vocal fold collision with high spatial and temporal resolution 11

Introduction 11

Development 14

Assumptions 14

Implementation 16

Validation 21

Mechanical stress during collision 26

Discussion 27

Chapter 3: Modeling mechanical stresses as a factor in the etiology of benign vocal fold lesions' 32

Introduction 32

Methods 33

Lumped mass model 33

Finite element model 38

Results 41

Discussion 47

Chapter 4: A theoretical investigation of the role of superficial lamina propria stiffness during voice production 51

Introduction 51

Methods 53

Results 58

Discussion 66

Chapter 5: Measurements of vocal fold collision forces during phonation 71

Introduction 71

Methods 73

Collision force sensor design, construction and characterization 73

Experimental setup 79

Experimental protocol 80

Data processing and analysis 81

Results 82

Discussion 87

Chapter 6: Contributions and proposed work 94

Method for theoretical study of vocal fold collision..... 94
Method for in vivo study of vocal fold collision 96
Support for mechanical injury of vocal fold tissue hypothesis..... 97
Measurement and interpretation of vocal fold collision forces 99
Future directions 100
Bibliography 101

LIST OF FIGURES AND TABLES

Figure 1.1: Vocal fold and air flow oscillation during voice production..... 2

Figure 1.2: Anatomy of human voice production. 3

Figure 1.3: Geometry of the vocal folds prepared for voice production. 8

Figure 2.1: Calculation of initial conditions for glottal closure using a finite element model of the vocal fold. 17

Figure 2.2: Finite element model of the membranous portion of a vocal fold during glottal closure. 20

Figure 2.3: Effect of subglottal pressure on the medial movement of the vocal fold as predicted by a finite element model of vocal fold collision..... 23

Figure 2.4: Effect of subglottal pressure on the area of contact between the vocal fold and the contact surface as predicted by a finite element model of vocal fold collision .. 24

Figure 2.5: Effect of subglottal pressure on the total contact force between the vocal fold and the contact surface as predicted by a finite element model of vocal fold collision 25

Table 2.1: Comparison between linear regression analysis of peak contact force and subglottal pressure for theoretical predictions using a finite element model and Jiang and Titze's (1994) experimental measurements on canine hemilarynges 26

Figure 2.6: Relationship between local contact force and mechanical stress on the medial vocal fold surface during collision as predicted using a finite element model..... 28

Figure 3.1: Development of a lumped mass model of vocal fold collision. 34

Table 3.1: Typical vocal fold dimensions and material properties from the literature..... 37

Table 3.2: Lumped model parameters in terms of biomechanical variables 37

Figure 3.2: Finite element model of vocal fold collision..... 39

Table 3.3: Effect of physiological parameter manipulation on compressive stress magnitude as predicted by a lumped mass model of vocal fold collision 42

Figure 3.3: Dependence of superficial stress in vocal fold tissue during collision and vocal fold vibration frequency (i.e. pitch) on geometric and material parameters as predicted by a lumped mass model of vocal fold collision..... 43

Figure 3.4: Effect of vocal fold collision on components of the stress tensor at the injury prone region for a driving pressure of 0.8 kPa as predicted with a finite element model..... 44

Figure 3.5: Spatial variation of stress tensor components in superficial tissue along the vocal fold edge for a driving pressure of 0.8 kPa as predicted by a finite element model..... 45

Figure 3.6: Dependence of stress tensor components in the injury prone region during collision on driving pressure as predicted by a finite element model..... 46

Figure 4.1: Finite element model of vocal fold closure and collision with four distinct tissue layers..... 54

Table 4.1: Material properties of vocal fold tissues used in a finite element model of vocal fold collision..... 56

Figure 4.2: Effect of SLP stiffness on vocal fold deformation in the midmembrous region at the start of glottal closure as predicted by a layered finite element model..... 60

Figure 4.3: Effects of SLP stiffness on the falling portion of the aerodynamic waveform as estimated by glottal area squared and glottal area as predicted by a layered finite element model..... 61

Figure 4.4: Effect of SLP stiffness on maximum contact force between the vocal folds and glottal area as predicted by a layered finite element model..... 62

Figure 4.5: Effect of SLP stiffness on maximum normal compression in the midmembranous region during vocal fold collision as predicted by a layered finite element model..... 63

Figure 4.6: Effect of SLP stiffness on maximum vertical shear stress on the plane parallel with the plane of collision (*zx*) in the midmembranous region during vocal fold collision as predicted by a layered finite element model..... 64

Figure 4.7: Effect of SLP stiffness on maximum longitudinal (*yy*) tension in the midmembranous region prior to vocal fold collision as predicted by a layered finite element model 65

Figure 5.1: Mechanical housing of sensor for measuring in vivo vocal fold collision forces and placement of the sensor between the vocal folds 74

Figure 5.2: Construction of the active area of a low profile force sensor for measuring vocal fold collision forces in vivo 75

Figure 5.3: Analog processing of signal from pressure sensitive piezoelectric film to produce voltage output that is proportional to force input 77

Figure 5.4: Voltage output of a low profile force sensor placed between human vocal folds during production voice 78

Figure 5.5: Production of voice by a subject while a low profile sensor is rested against his one rigid fold 84

Figure 5.6: Segment of simultaneously acquired intraglottal force, EGG and audio data during voice production. 85

Table 5.1: Regression analysis of vocal fold collision force as a function of voice frequency and voice intensity (subject 1) 86

Table 5.2: Regression analysis of vocal fold collision force as a function of voice frequency and voice intensity (subject 2) 87

Figure 5.7: Scatter plots of vocal fold collision force, voice intensity and voice frequency data points measured in two male subjects 88

This thesis is dedicated to Professor Thomas A. McMahon (1943-1998), who opened my eyes to the intriguing relationship between solid mechanics and voice production

ACKNOWLEDGEMENTS

Thank you to all who helped to make this thesis a reality. I am appreciative of a graduate fellowship from the Whitaker foundation that has supported me during my final five years of graduate study and of scholarships from the Alberta Heritage Scholarship Fund, the Canadian Federation for University Women and the Harvard Division of Engineering and Applied Sciences that contributed to my initial year of graduate study.

I am indebted to Professors Robert D. Howe (Harvard Division of Engineering & Applied Sciences), Robert E. Hillman (Massachusetts Eye and Ear Infirmary) and Kenneth N. Stevens (Massachusetts Institute of Technology Department of Electrical Engineering & Computer Science) who have helped to transform me from a fledgling graduate student into a young researcher. These faculty members along with Professor John Hutchinson (Harvard Division of Engineering & Applied Sciences) helped to sculpt this scientific work from its early overly ambitious state into its current form. The insights of informal advisors have also left their mark on this document. Markus Hess (Hamburg University) shared fascinating thoughts about vocal tissue injury and his

experiences measuring impact forces with me. Jim Kobler (Massachusetts Eye and Ear Infirmary) lent his creativity to experimental design and proof reading skills to manuscript drafts on numerous occasions. Dr. Steven Zeitels (Massachusetts Eye and Ear Infirmary) welcomed me into the operating room so that I could learn about surgical aspects of voice treatment and lent his manual dexterity to the placement of the vocal fold impact force sensor. The generous and enthusiastic participation of five individuals in my vocal fold collision experiments inspired me to try to make contributions to the fields of speech pathology and laryngology.

Many others also contributed to the work contained in the pages that follow. Jim MacArthur (Harvard Division of Engineering & Applied Sciences) and Stan Coutreau (Harvard Department of Physics) offered invaluable advice and assistance with the design and assembly of the sensor. Cami Lau, Jaime Lee and Philippe Bouzaglou took time out of their undergraduate studies to lend a hand prototyping sensors, extracting finite element data and constructing finite element models.

On a personal note, I am grateful to my friends and family who have kept me sane throughout the past six years. Mom & Dad – you have always been a phone call or e-mail away in times of frustration. Thank you for gently pushing me on the track when I became distracted by other pursuits. Josh – you've been my sounding board, therapist, and companion through the highs and lows. Thank you for being supportive, keeping me grounded and making me smile.

CHAPTER 1: INTRODUCTION

The human vocal apparatus and its control capabilities are unique in the animal kingdom and enable our exceptional abilities to speak and sing. In addition to the importance of daily communication in our personal lives, an estimated 23% of people in the workforce have occupations in which voice use is essential (Titze et al., 1997). Pathologies of the speech system may increase the effort needed to speak, decrease the quality of sound produced, cause pain, or eliminate the ability to speak.

Voice is produced through a coupled oscillation between folds of tissue called the vocal folds and the airflow between them (Figure 1.1). When the folds are brought together to the midline and there is a sufficient, but not excessive, pressure buildup in the lungs, the coupled oscillation ensues. The tissue oscillation can be observed using endoscopic techniques. The aerodynamic oscillation is a sound wave that is filtered by the rest of the vocal tract, including the pharynx, oral, and nasal cavities, to generate the sound heard by an observer (Figure 1.2). This method of sound production is used in the production of vowels and some consonants, and is the foundation of pitch contours.

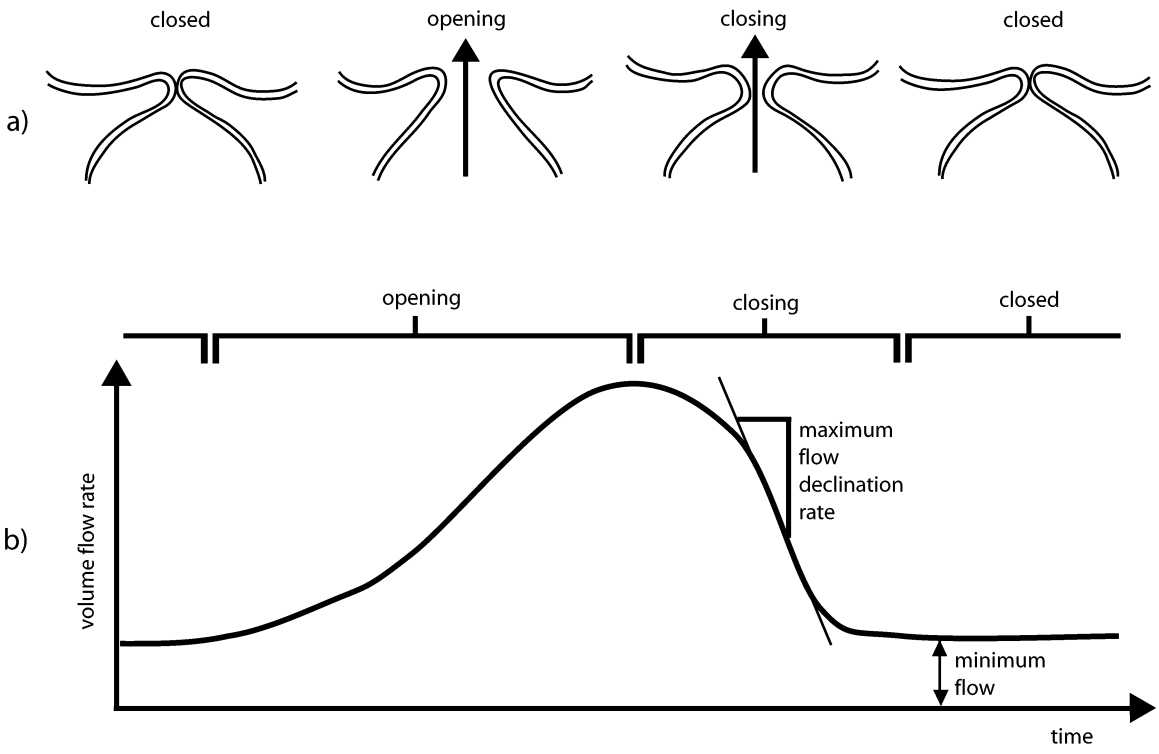

Figure 1.1: Vocal fold and air flow oscillation during voice production.
(a) Coronal sections through the larynx showing the medial profile of the vocal folds during one cycle of vibration. The double lines are the medial contours of the two vocal folds. The spaces between the double lines are continuous with the airway. Arrows indicate airflow between the vocal folds. Opening is caused by air pressure below the vocal folds. Closing is caused by decreased air pressure between the vocal folds and elastic recoil of the tissue. **(b)** Plot of volume airflow between the vocal folds during one cycle of vibration. Air pressure beneath the vocal folds and vocal fold configuration govern the airflow between the vocal folds. The parameters maximum flow declination rate and minimum flow are associated with voice quality.

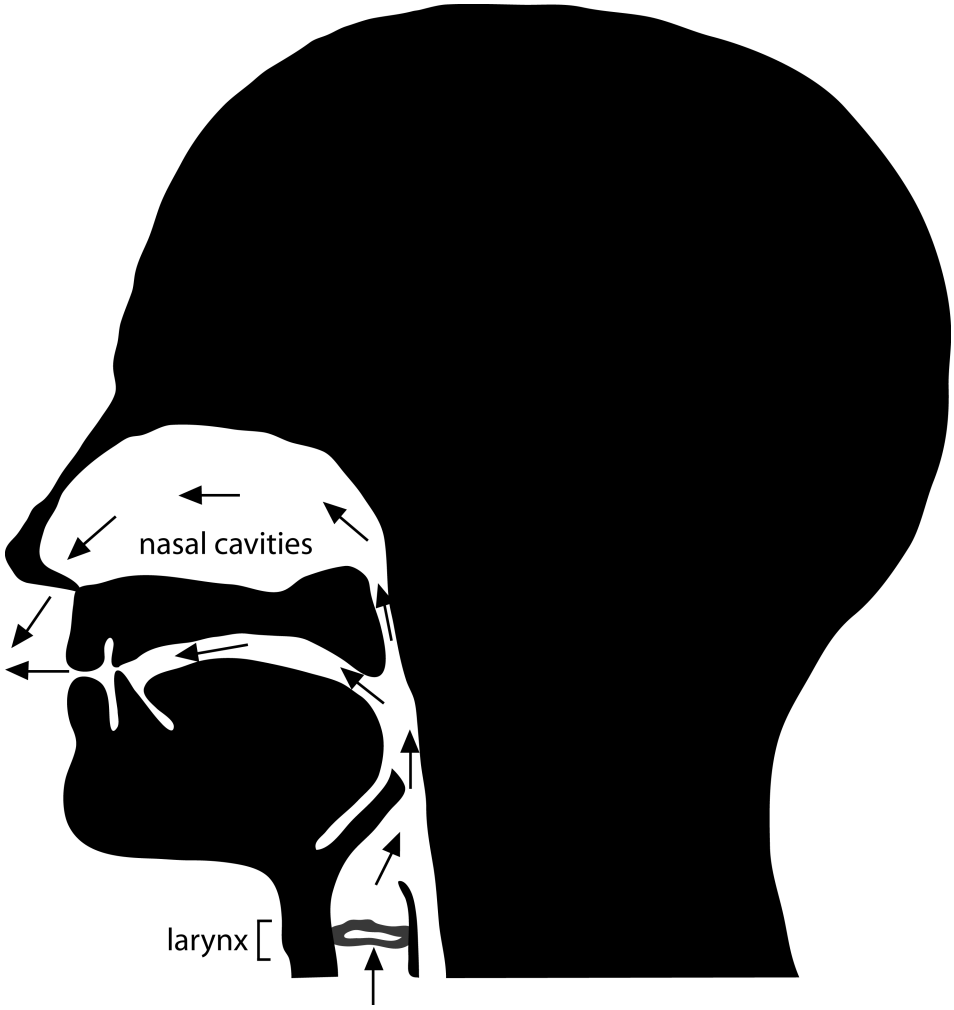

Figure 1.2: Anatomy of human voice production.
The vocal folds are sketched in gray and are located in the larynx. During voice production air moves from the lungs, between the vocal folds, through the oral and nasopharynx, and out of the mouth and nostrils as shown by the arrows.

Vocal fold tissue mechanics affect perceived voice by contributing to the shape of the aerodynamic wave form, especially the decreasing portion, as explained by the myoelastic-aerodynamic theory of voice production (Jiang et al., 2000). Air pressure forces on the inferior and medial aspects of the adducted vocal folds cause separation of the vocal folds and gradually increasing airflow between the vocal folds (the opening phase). Maximum opening represents a balance between the pressure of the air flowing between the folds, which acts laterally, and elastic forces within the deformed vocal folds, which act medially. When air pressure drops due to flow acceleration, elastic forces dominate and cause the tissue to recoil towards its neutral position (the closing phase). This is accompanied by decreased airflow between the vocal folds. The vocal folds collide as they move past their neutral positions, and air pressure in the lungs builds up to cause them to separate and initiate another cycle. Growths on the surface of the vocal folds, such as vocal nodules, vocal polyps and neoplasias affect vocal fold closure by altering minimum flow and maximum flow declination rate, which are variables that characterize the decreasing flow section of the aerodynamic waveform (Hillman et al., 1989). The influence of vocal fold mechanics on voice quality is further illustrated by the successful use of surgical modifications to vocal fold tissue to restore voice quality that has been negatively impacted by the presence of organic vocal fold pathologies such as nodules, polyps and scar (Zeitels et al., 2002).

In addition to contributing to voice production, vocal fold mechanics contribute to vocal fold injury. Specifically, the closure and collision phase of the voice production cycle has been implicated as a cause of pathology development (Titze, 1994). The deformations in vocal fold tissue during the collisions between them result in mechanical

stresses that are proposed to cause mechanical and functional tissue injury that manifests as benign vocal fold pathologies such as vocal nodules. The pathologies observed are 1-2mm in size and involve the thickness of the lamina propria (Dikkers, 1994). Therefore it is likely that mechanical stress changes occur on a similar or smaller scale. The stresses that are likely to be associated with collision and cause tissue damage include compressive stress perpendicular to the plane of contact that may cause cellular rupture, and shear stress parallel to the plane of contact that may cause separation of tissue elements. Damage may also be caused by alterations in cellular function in response to environmental stresses. However, it is not clear which components of stress govern cellular function. Von Mises stress may be a quantity that is suitable for evaluating cellular deformation. It is a scalar quantity that represents distortion energy and whose magnitude is a predictor of failure in engineering materials (Chandrupatla and Belegundu, 1997).

Simple and complex theoretical models have been used to quantify mechanical stress in vocal fold tissue. Titze (1994) uses impact/momentum principles and empirical relationships between vocal fold structure and function to generate an order of magnitude estimate of collision-induced compressive stress. The inputs do not relate directly to tissue structure, and the output is limited to one spatial invariant component of the stress tensor. Jiang et al. (1998) use finite element models to examine the spatial variation of tissue stress levels. They restrict their analysis to the case of natural vibration, examine one stress invariant and do not examine stress dependence on geometric and material parameters. Other models of voice production have not been used to predict tissue stress. Lumped mass models of voice production that were developed for speech synthesis

applications and subsequently used for quantitative study of voice physiology (Story and Titze, 1995;Wong et al., 1991) have not interpreted spring deformation as an indicator of stress. Finite element models of voice production (Alipour et al., 2000) have neither sufficient spatial resolution nor an appropriate three-dimensional mesh to examine stress variations on the submillimeter scale of vocal fold pathology. Jiang and Titze (1994) and Hess et al. (1998) cite the impact stress hypothesis as their motivation for identifying situations that increase intra-fold collision forces and implying corresponding increases in mechanical stresses. The relationship between measured total collision forces and distributed mechanical stresses remains to be defined. The work presented in this thesis builds on these efforts by developing new theoretical models of vocal fold mechanics with high spatial resolution, developing a new method of measuring vocal fold collision forces during voice production in humans, and applying these methods to the study of mechanical stress levels in vocal fold tissue.

MECHANICS OF VOCAL FOLD TISSUE

The mechanical behavior of vocal fold tissue has implications for voice production and vocal fold pathology development. In order to apply principles of solid mechanics to gain insight to these topics it is necessary to understand the mechanical details of vocal fold tissue including its geometric dimensions, material properties, boundary conditions and applied loads.

A resting vocal fold is a three dimensional structure with outer dimensions of 1- 2 cm in length, 0.5 – 1 cm in width and 0.5 – 1 cm in height (Titze and Talkin, 1979). It protrudes into the middle of the airway such that the longitudinal dimension spans the diameter of the larynx. The superior, inferior and medial faces are unconstrained. The

anterior, posterior and lateral faces are fixed to laryngeal cartilages (Figure 1.3). It is composed of tissue layers. The epithelium is the outermost layer on the three exposed faces and is 0.1 mm thick. In longitudinal tension it is strain stiffening, and characterized by a Young's modulus of 41.9 kPa for strains of less than 15% (Alipour-Haghighi and Titze, 1991). Beneath the epithelium lies a 0.5 mm thick layer called the lamina propria (Hirano et al., 1983). It is a soft, gel like substance that is viscoelastic and shear thinning with a shear modulus on the order of 100 Pa and a dynamic viscosity on the order of 1 Pa-s at 1 Hz (Chan and Titze, 1999a). Beneath the lamina propria, forming the bulk of the vocal fold interior is the thyroarytenoid muscle, which is characterized in longitudinal tension by a Young's modulus of 20.7 kPa for strains of less the 15% and higher moduli for higher strains (Alipour-Haghighi and Titze, 1991). At their medial aspects, the muscle and the lamina propria are separated by the vocal ligament. This string like structure is approximately 0.3 mm thick (Hirano et al., 1983) and demonstrates strain stiffening behavior in longitudinal tension that can be approximated by a Young's modulus of 36.1 kPa (Min et al., 1995).

During voicing the vocal folds undergo static and dynamic deformations. The vocal folds are statically stretched 10 % in the process of being moved into a voice producing configuration (Hirano et al., 1988). Additional static strains are imposed through the actions of extrinsic laryngeal muscles in order to manipulate pitch and vocal register. During voice production the center of the medial surface of the vocal folds deforms approximately 1 mm laterally during each vibration cycle, which occurs approximately 150 times per second to produce voice at 150 Hz (Zemlin, 1997). Theoretical extensions of frequency dependent behavior of the lamina propria suggest that it is almost purely

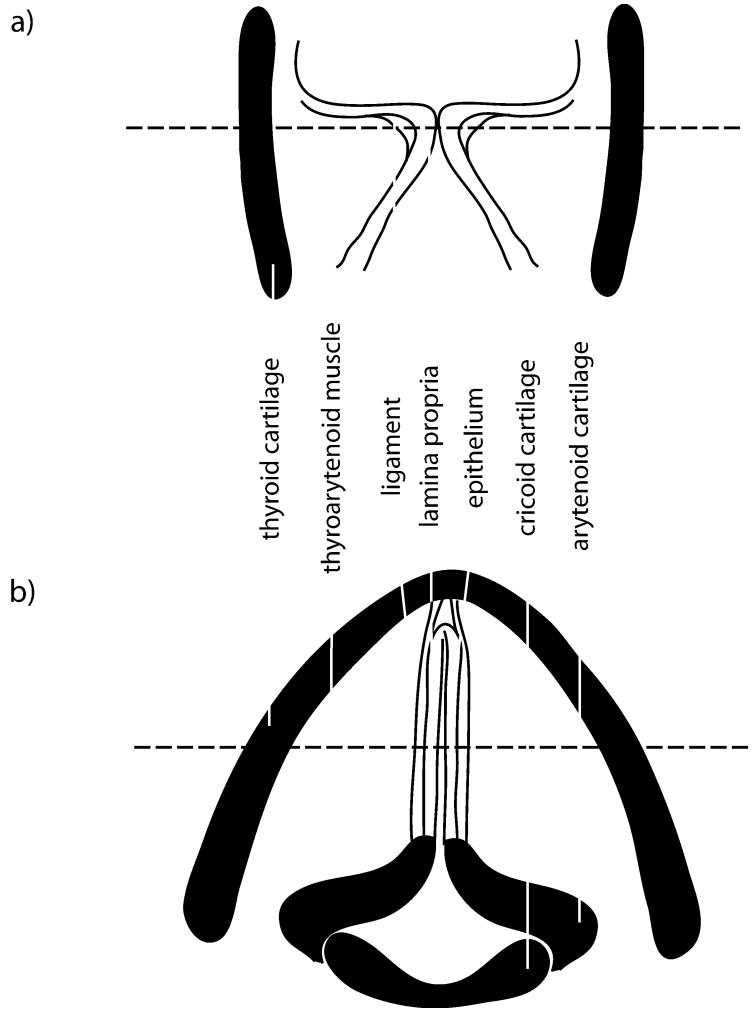

Figure 1.3: Geometry of the vocal folds prepared for voice production.
The laryngeal cartilages are indicated by solid black structures. **(a)** coronal section through the larynx illustrating the four soft tissue layers in the two vocal folds bounded by the thyroid cartilage. The dashed line indicates the section cut for the lower figure. **(b)** transverse section through the larynx. The arytenoid cartilages swivel on the cricoid cartilage to bring the edges of the vocal folds together. The dashed line indicates the section cut for the upper figure

elastic at voicing frequencies (Chan and Titze, 2000). There are no data on the behavior of the other materials during high frequency deformation, nor are there data on their behavior in compression or transverse tension. Such data would be experimentally challenging to obtain given the small size of vocal fold tissue samples.

The vocal fold vibration cycle is maintained through loads applied to the tissue by air pressure and the opposing fold. Tracheal puncture methods estimate air pressure 2 cm beneath the vocal folds (i.e. subglottal pressure) on the order of 1 kPa (Lieberman, 1968). Air pressure between the vocal folds can be measured using an in vitro hemilarynx set up (Jiang and Titze, 1993). Such preparations have been used to show that air pressure is at a maximum as the folds are separating and decreases as they move towards each other and collide (Alipour et al., 2001). The same preparation has been used to measure collision forces between the folds on the order of 10 mN and dependent on subglottal pressure (Jiang and Titze, 1994). In vivo measurements of collision forces in humans report difficulty maintaining good voice quality during the measurements (Hess et al., 1998).

RESEARCH OBJECTIVES AND THESIS ORGANIZATION

This thesis explores the mechanics of human vocal fold tissue during voice production using experimental and theoretical approaches. These efforts extend previously published theoretical models by collecting mechanical data in human subjects for use in model validation and creating models with high spatial resolution that represent the closure and collision part of the vocal fold vibration cycle.

The novel contributions are presented in four chapters. Chapter 2 details the development and validation of a finite element model of vocal fold tissue during voice production. This model of the closure and collision portions of vocal fold vibration is used to relate collision force and tissue stress, which may be a determinant of tissue injury. Chapter 3 examines the proposed mechanical etiology of vocal fold tissue lesions during voice production using this finite element model and a simpler lumped mass model. The results support the impact stress hypothesis of vocal nodule development. Chapter 4 details the development and validation of a finite element model of vocal fold tissue with four distinct tissue layers and use of this model to investigate the role of the soft superficial lamina propria layer. Results indicate that superficial lamina propria stiffness is a determinant of mechanical stress levels and voice quality. Chapter 5 reports experimental measurements of vocal fold collision force in humans. These measurements characterize the mechanical environment of vocal fold tissue, provide empirical relationships between force, pitch and volume and are useful for validating theoretical models of tissue mechanics. Each of these chapters includes a review of pertinent literature. A final chapter summarizes the contributions of the thesis and comments on possible future directions.

CHAPTER 2: A MECHANICAL MODEL OF VOCAL FOLD COLLISION WITH HIGH SPATIAL AND TEMPORAL RESOLUTION[1,2]

INTRODUCTION

A detailed theoretical model of vocal fold tissue mechanics during collision that connects tissue damaging variables with clinical or experimental variables and vice versa is an excellent tool with which to clarify the impact stress hypothesis (Chapter 1). A model of vocal fold collision that captures the dynamics of vocal fold closure also has the potential to be applied to prediction of the surgical outcomes by predicting the tissue correlates of the aerodynamic variables minimum flow and maximum flow declination rate, which relate to voice quality perceptions (Holmberg et al., 1988).

The idea to represent vocal fold tissue mechanics mathematically is not a new one. The simplest models represent the vocal folds using the basic mechanical elements (i.e. masses, springs and dampers) and were initially developed for speech synthesis

[1] Portions of this work were presented in "Analysis of Factors Affecting Vocal Fold Impact Stress Using a Mechanical Model" 142nd meeting of the Acoustical Society of America, Ft. Lauderdale, FL, December 2001

[2] This work is published as Gunter, H. E. (2003), "A mechanical model of vocal fold collision with high spatial and temporal resolution," Journal of the Acoustical Society of America. 113, 994-1000.

applications. The classic example uses two masses to represent a single vocal fold (Ishizaka and Flanagan, 1972). Variations by Story and Titze (1995), Wong et al. (1991) and Titze (1973;1974) incorporate additional masses to provide resolution in the depth and longitudinal dimensions. Story and Titze predict intraglottal collision pressures based on the deformation of the collision spring element that agree qualitatively with Jiang and Titze's (1994) experimental measurements. However, their peak pressure prediction is approximately five-fold less than the comparable experimental measurement (Jiang and Titze, 1994). The computational simplicity of these tissue mechanics models makes them an excellent foundation for the exploration of complex theories of voice aerodynamics (de Vries et al., 2002;Pelorson et al., 1994). Analysis using nonlinear dynamic techniques (Jiang et al., 2001b;Wong et al., 1991) provides some insight into origins of pathological voice. However, the spatial resolution of the lumped mass models is insufficient to reflect the scale of pathology and surgery, and their empirically assigned spring, damper, and mass values have few direct implications for vocal fold tissue physiology. This limits their applicability to the study of vocal fold tissue mechanics. Recently Titze & Story (2002) developed rules relating the lumped mass parameters to muscle activation levels. While this improves the physiological relevance, the spatial resolution remains low and therefore this model is not suited to the study of vocal fold tissue mechanics.

Continuum approaches represent the vocal folds more realistically at the expense of computational efficiency. To maintain computational time within a reasonable range these models require simplification of either the solid or fluid mechanics representation. Use of simplified two dimensional (Ikeda et al., 2001) or three dimensional beam (Berry

and Titze, 1996;Titze and Strong, 1975) geometries in analytical models does not capture the subtleties of vocal fold tissue anatomy. Numerical approaches permit the use of realistic three dimensional geometries (Titze and Talkin, 1979)). The numerical technique of finite elements has been used to create models that overcome the barriers of low spatial resolution and restricted geometries (Alipour et al., 2000;Jiang et al., 1998;Lobo and O'Malley, 1996). These techniques involve spatially and temporally discretizing a continuum mechanics problem into solid elements and time increments followed by numerical solution. In order to maintain computation at reasonable levels these have used spatial resolution that is inadequate for the study of tissue mechanics. Alipour et al.'s (2000) self-oscillating model requires increased spatial resolution, calculation of mechanical stress distributions and extension to true three-dimensionality in order to represent vocal fold pathologies and examine mechanical stress distributions. Jiang et al.'s (1998) and Lobo and O'Malley's (1996) finite element models of vocal fold tissue have sufficient spatial resolution to represent pathology, but limit analysis to resonant and forced vibration. They require an explicit representation of collision forces between the vocal folds in order to be used in investigations of contact related pathology etiologies and voice quality. Variations on these finite element models have the potential to be excellent tools with which to investigate vocal fold tissue mechanics.

A finite element model of vocal fold collision that is not self oscillating is presented below. It has spatial resolution that is capable of representing the submillimeter scale of vocal fold injury and repair, temporal resolution that captures the submillisecond time scale of vocal fold collision and an explicit representation of vocal fold collision. Model predictions of collision force are validated against experimental data and model potential

is illustrated in an examination of the relationships between collision force and mechanical stress levels.

DEVELOPMENT

Assumptions

The model of vocal fold collision presented below has three unique features. The spatial resolution of 250 μm is finer than that incorporated in other vocal fold models. A single isotropic, linear elastic material characterizes the entire vocal fold structure. Glottal closure during phonation is represented using a non-oscillating model consisting of appropriate initial conditions and a high fidelity model of vocal fold solid mechanics. Justifications for these features are outlined below.

The necessary spatial resolution is dictated by the size of geometric variations in the model, the desired resolution of model outputs, and desired computational speed. The model is intended for use in studying the effects of vocal fold pathologies and their repair on tissue movement and for investigating the distribution of mechanical stresses in vocal fold tissue as an indication of pathology development risk. Benign vocal fold pathologies such as nodules and polyps have dimensions of 1-2 mm on the vocal fold surface (Dikkers, 1994). Spanning the pathology with a minimum of four elements requires element dimensions of 250 μm and allows for some sculpting of the geometry. Surgical repair of the vocal fold can involve manipulation of only the superficial lamina propria (Zeitels, 1998), which, at approximately 500 μm thick (Hirano et al., 1983), can be represented by two elements. Mechanical stresses that are important in tissue injury are on the same scale as or smaller scale than the pathologies that they are proposed to cause.

Therefore a resolution that is sufficient to represent pathologies provides appropriate information on stress distributions. Further resolution would increase geometric fidelity and output detail, but would also increase computational load significantly.

A simple material definition is used in the model. The assumption of linear elasticity is consistent with Min et al.'s (1995) observation of linear stress-strain behavior of human vocal ligaments for strains of less than 15%. Strains in the model do not exceed this 15% upper bound. The primary mode of deformation of the vocal fold during vocal fold closure is compressive in the transverse (i.e. medial-lateral and inferior-superior) directions. However, there is a lack of direct data on the elastic properties of vocal fold tissue when undergoing this kind of deformation. Therefore parameters based on tissue behavior during longitudinal tension are used to characterize the material properties. The range of elastic moduli derived by Min et al. (1995) using human vocal ligament samples (21.2 kPa-42.2 kPa) spans the moduli derived by Alipour-Haghighi and Titze (1991) for unstimulated canine thyroarytenoid muscle (20.7 kPa) and canine vocal fold cover (41.1 kPa) and are the same order of magnitude as moduli derived by Kakita et al. (1981) using canine vocal fold muscle and cover. The assumption of homogeneous properties is within the spread of the data in the literature.

Some studies suggest that air pressure in the glottis is low during glottal closure. The myoelastic-aerodynamic theory of voice production cites three reasons for glottal closure: elastic recoil of the deformed tissue, decreased pressure on the glottal walls due to the high velocity of the air stream through the opening and decreased subglottal pressure (Jiang et al., 2000). Experimental measurements performed on canine hemilarynges illustrate that, in an almost fully adducted larynx, air pressure in the glottis remains below

10% of subglottal pressure during glottal closure and does not rise until full closure has occurred (Alipour and Scherer, 2000). Measurements performed on excised human hemilarynges also demonstrate reduced glottal air pressures during closure (Alipour et al., 2001). It is consistent with observations of minimum air pressures and maximum vocal fold deformation when the glottis is fully open to postulate that elastic forces dominate during glottal closure, and to focus on these forces in a model of glottal closure.

Implementation

The model geometry represents the membranous portion of a fully adducted single vocal fold (Figure 2.1). The model is defined in Cartesian coordinates. The origin is in the midposterior glottis, inferior to the bulge of the vocal fold. The *y* axis defines the midline of the glottis, *x* dimensions indicate lateral distance from the glottal midline, and *z* translations represent movement in the vertical direction. The vocal fold dimensions are 1.4 cm long (*y* direction), 0.5 cm wide anteriorly, 1.0 cm wide posteriorly (*x* direction), and 1 cm high posteriorly (*z* direction). The anterior, posterior and lateral surfaces are fixed to represent their attachment to the laryngeal cartilages. This structure is based on Titze and Talkin (1979) and uses their nominal parameters (i.e. shaping factor (*s*) equal to 0.05 radians, glottal angle (*w*) equal to 0 radians and inferior surface angle (*q*) equal to 0.7 radians). The Titze and Talkin geometry is modified by applying a fillet with a radius of 0.05 cm to the superior medial curve in order to create a smooth contour in the coronal plane. The glottal width (*g*) between the inferior aspect of the fillet and the superior aspect of the inferior surface is derived from an expression given by Titze and Talkin:

$$g(0.05 \le h \le 0.5) = 0.45 - 1.9(h - 0.5) + 2(h - 0.5)^2 \qquad (2.1)$$

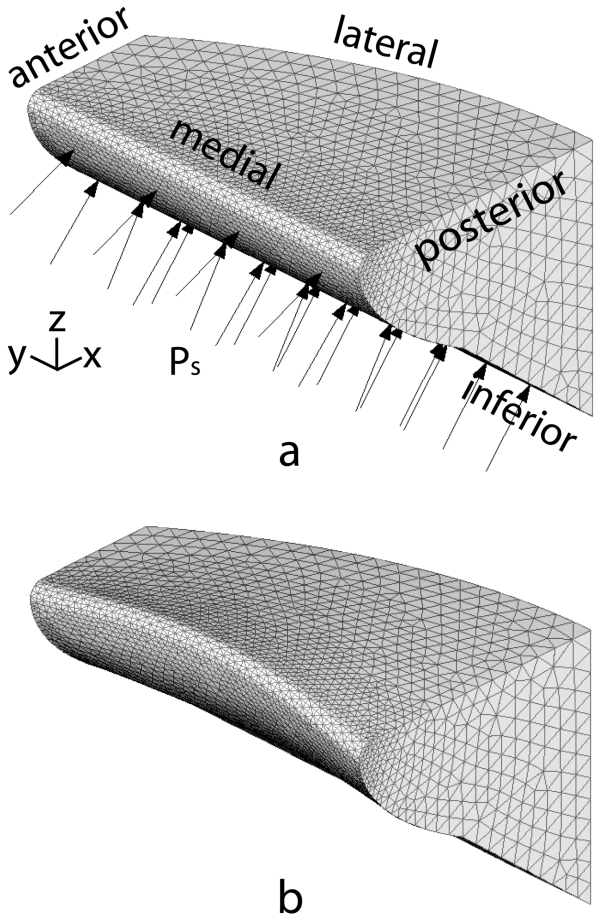

Figure 2.1: Calculation of initial conditions for glottal closure using a finite element model of the vocal fold.
(a) Problem formation: the three dimensional solid represents the undeformed vocal fold. Triangular divisions indicate individual three-dimensional finite elements. Anterior, lateral and posterior boundaries are held fixed. The arrows indicate the direction and location of application of forces representing subglottal pressure (P_s). **(b)** Problem solution: the three dimensional solid represents the deformed vocal fold. This output is dependent on subglottal pressure and is the initial condition for glottal closure (see Figure 2.2).

h is the vertical distance below the superior surface. The minimum glottal width of 0.0 cm that occurs at the inferior end of the fillet (*h* equal to 0.05 cm) indicates that the undeformed vocal fold is tangent to the glottal midline. A similar geometry has been used by Alipour et al. (2000) with good results.

A finite element support software package (Femap 8.0; EDS inc; Plano, Texas.) is used to divide the geometry into 14242 three-dimensional tetrahedral elements, which provides an elemental resolution of 250 μm on the medial surface. The model has 23637 nodes, which reflect the ten nodes necessary to define each element and provide 70911 degrees of freedom. Repetition of analyses using a model with 2.5 fold fewer elements affects collision force predictions by a maximum of 4%, which indicates that the mesh is fine enough to achieve convergence of results.

A common material defines all elements in the model. The material properties are non-directional and linear, with a Young's modulus (E) of 36.1 kPa and a Poisson's ratio (ν) of 0.3. These parameters are based on experimental measurements on human vocal ligament samples by Min et al. (1995) and are valid for strains of less than 15%. None of the simulations presented below produce strains greater than this magnitude. The first mode of vibration is calculated using a linear perturbation eigenvalue analysis of the vocal fold geometry in the absence of the pressure load and contact condition (Abaqus Standard 5.8.1; Abaqus inc.; Pawtucket, RI) to provide an evaluation of the geometric and material representation.

Interaction between the vocal fold and a rigid surface in the middle of the glottis (i.e. a *yz* plane at $x = 0$) represents the interaction between the modeled fold and the opposing

vocal fold. This surface and the nodes on the medial surface of the vocal fold form a contact pair: As a medial surface node becomes coincident with the rigid surface, sufficient force is applied to prevent the node from passing through the surface. Contact forces are in the *x* direction since the interaction is frictionless. Total contact force is the sum of the forces acting on all medial surface nodes. Contact area is a function of the number of nodes that are in contact with the surface. When the vocal fold it in its neutral position the contact area is 7 mm^2.

Deformation of the vocal fold model due to subglottal pressure (P_s) defines the initial condition for vocal fold closure. A distributed load applied perpendicularly to the element faces that form the inferior and medial surfaces represents subglottal pressure (Figure 2.1a). Equilibrium tissue deformation (Figure 2.1b) and stress distributions, calculated for each subglottal pressure (P_s= 0.4, 0.6, 0.8, 1.0, 1.5 and 2.0 kPa) (Abaqus Standard 5.8-1), define the maximally open glottis. Geometric nonlinearities are accounted for during this calculation.

Vocal fold closure is the progression from maximally open to fully closed (Figure 2.2) glottis due to elastic forces within the tissue. The nonlinear, transient, dynamic solution for a given initial condition is obtained by incrementing forward through time using implicit integration algorithms (Abaqus Standard 5.8-1). Time increments that result in solution convergence, calculated based on the half step residual and changes in the contact state, range from 10-100 μs before collision occurs and 10-100 ps during collision. Typically between 50 and 100 increments are necessary to predict 3ms of tissue movement and capture complete vocal fold closure. Outputs of these calculations

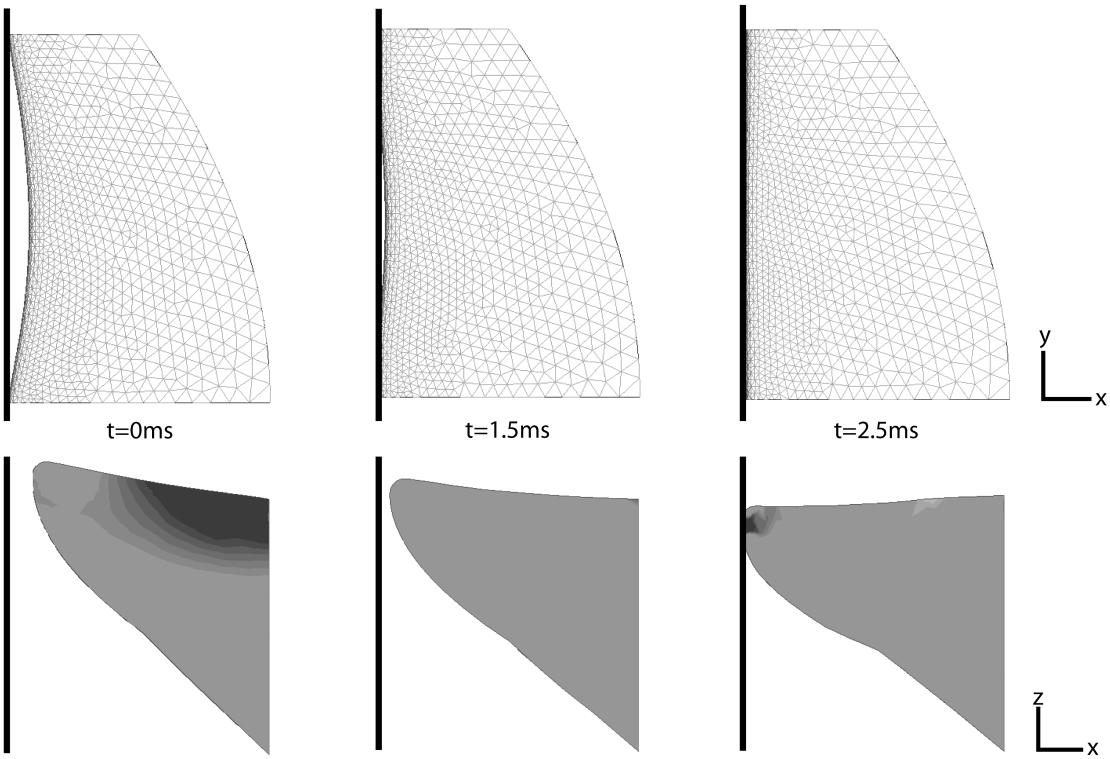

Figure 2.2: Finite element model of the membranous portion of a vocal fold during glottal closure.
Each column provides two views of the model at one time increment. The vertical lines represent the plane of contact with the opposing vocal fold. Images in the top row are superior views, similar to those obtained clinically using a laryngoscope, that illustrate the changing glottal area. The bottom row of images are coronal sections through the mid-membranous region of the vocal fold. The degree of dark shading in the bottom row of images represents the magnitude of compressive stress in the tissue in the direction perpendicular to the plane of contact. The images in the left hand column represent the initial condition. The deformation is due to the application of a subglottal pressure of 2 kPa. There are compressive stresses in the superior lateral region with a maximum magnitude of 3.5 kPa. This provides the elastic energy that causes the fold to move. The middle and right hand columns show frames in the solution. The images in the middle column represent the deformation of the vocal fold 1.5 ms after the start of glottal closure. There are no compressive stresses greater than 3 kPa. The images in the right hand column represent the deformation of the vocal fold 2.5 ms after the start of glottal closure. There is a compressive stress concentration with a magnitude of 10 kPa at the site of contact with the opposing fold.

include movement of each node, mechanical stresses in each element, and interactions between nodes and the rigid midline surface.

The goals with this model are to validate predictions of closure kinematics and collision surface forces against published experimental measurements and to examine the relationship between collision surface forces and mechanical stress levels in the tissue during collision. Model predictions that reflect these goals are discussed below.

VALIDATION

The natural frequency is 127 Hz, which is consistent with experimentally measured resonant frequencies (Kaneko et al., 1987) and theoretically predicted resonant frequencies for adult male voices (Alipour et al., 2000). This agreement corroborates the geometric and material definitions.

Glottal closure dynamics are an important output of the model, and model behavior agrees with observations of vocal fold vibration. The qualitative movement of the fold includes movement towards the midline and collision with the opposing fold (Figure 2.2). Closure begins at the anterior and posterior ends and progresses towards the mid-membranous region (Figure 2.2, top row), which is consistent with in vivo stroboscopic observations of fully adducted phonation. The initial mid-membranous glottal displacement (i.e. the maximum lateral displacement of the medial vocal fold edge) is an approximately linear function of subglottal pressure and ranges between 0.15 mm and 0.8 mm (Figure 2.3). These predictions are consistent with previous visual observations of normal vocal fold vibration (Zemlin, 1997). The inferior portion of the vocal fold edge is the first point of collision with the opposing fold. As collision proceeds, contact includes

the superior vocal fold edge (Figure 2.2, bottom row). This progression is similar to phase differences that are observed clinically. Contact areas, which are calculated based on the number of nodes touching the midline surface in the vocal fold closure and collision solutions, are also functions of P_s and time (Figure 2.4). The contact areas range from 0 to 35 mm^2, which lies within the area of vocal fold contact imaged by Jiang and Titze (1994).

Collision dynamics during closure are another important output of the model, and model behavior agrees with published experimental results. The total collision force increases with time and reaches either a peak or a plateau depending on the initial P_s (Figure 2.5). The rise time of collision in a 3 mm mid-membranous region for P_s=1.5 kPa and 2.0 kPa is approximately 0.5 ms, which is equal to the experimentally measured rise time for impact with a 3 mm diameter central sensor as measured in canine hemilarynges by Jiang and Titze (1994). Due to the collision force plateau, there are no clear force peaks for P_s less than 1.5 kPa. Collision force peaks are defined either as the force magnitude at the time of full closure, which is independent of P_s (Figure 2.3), or as the force magnitude at the time of maximum contact area, which is dependent on P_s (Figure 2.4). These peaks are used to derive linear relationships between subglottal pressure and peak collision force. Table 2.1 compares the slopes and regression coefficients for lines fit to model predictions with those fit to in vitro experimental data collected from canine hemilarynges by Jiang and Titze (1994). Both definitions of theoretical peak collision force fall within the span of the experimental results.

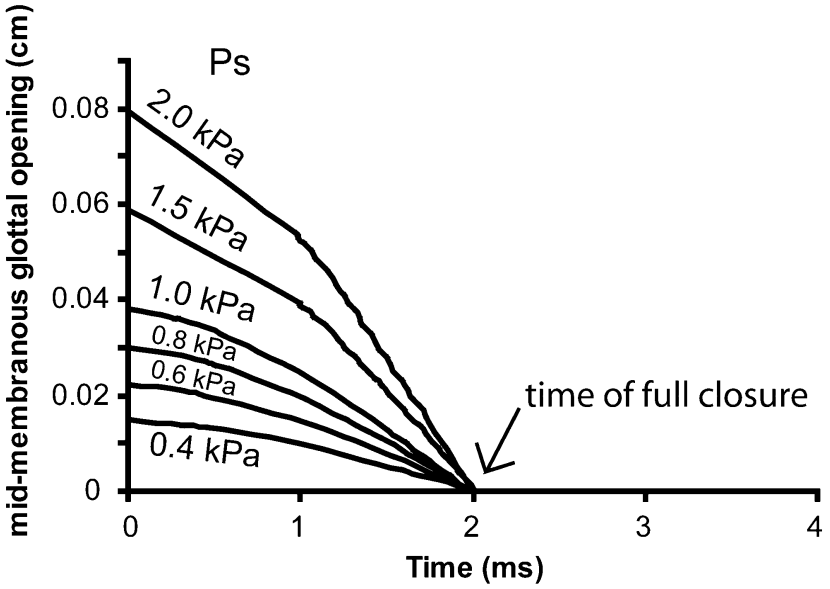

Figure 2.3: Effect of subglottal pressure on the medial movement of the vocal fold as predicted by a finite element model of vocal fold collision
Each line traces the solution for the *x* position of a mid-membranous point on the medial edge of the vocal fold edge during glottal closure in a single model. The models differ by the subglottal pressure magnitude used to calculate the initial closure condition (i.e. t = 0). The arrow points to the time when the mid-membranous glottal opening and glottal area are zero, which is defined as the time of full closure. This value is not dependent on subglottal pressure.

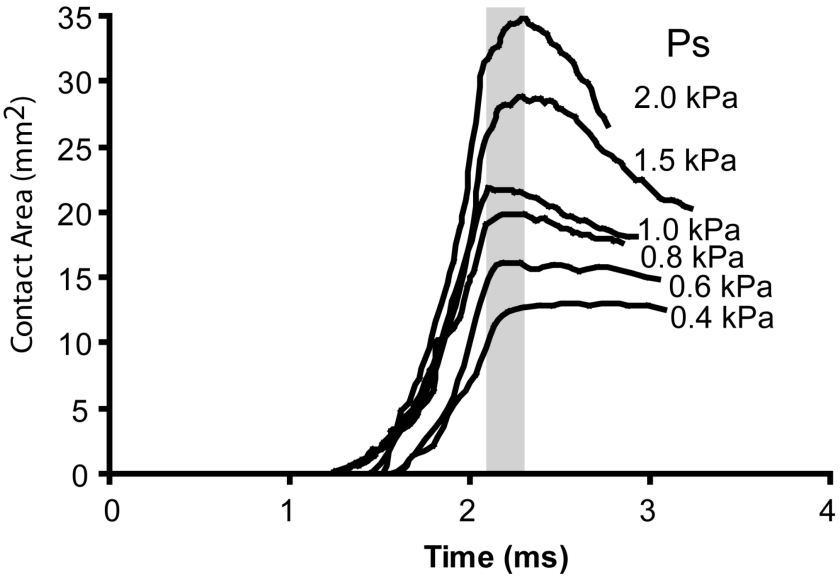

Figure 2.4: Effect of subglottal pressure on the area of contact between the vocal fold and the contact surface as predicted by a finite element model of vocal fold collision
Each line traces the solution for contact area, which is proportional to the number of nodes that are at $x = 0$ (i.e. touching the contact plane) during glottal closure in a single model. The models differ by the subglottal pressure used to calculate the initial condition of glottal closure (i.e. $t = 0$). The shaded area indicates the temporal range of contact area maxima, which varies among models.

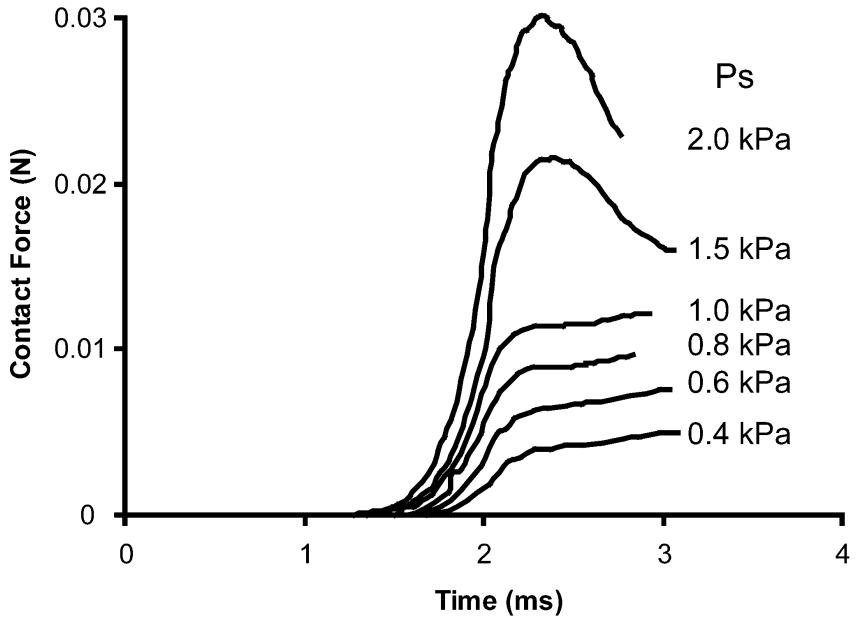

Figure 2.5: Effect of subglottal pressure on the total contact force between the vocal fold and the contact surface as predicted by a finite element model of vocal fold collision Each line traces the solution for contact force, which is the sum of point loads applied by the contact plane to nodes on the medial surface, during glottal closure in a single model. The models differ by the subglottal pressure magnitude used to calculate the initial condition of glottal closure (i.e. $t = 0$).

Table 2.1: Comparison between linear regression analysis of peak contact force and subglottal pressure for theoretical predictions using a finite element model and Jiang and Titze's (1994) experimental measurements on canine hemilarynges

Contact Force Definition	Linear Slope (mN / kPa)	Regression Coefficient
Model prediction – peak contact area	16.39	0.977
Model prediction – full closure	10.48	0.930
Experimental measurement (Jiang and Titze, 1994)	Range =7.70 - 26.60 Mean =12.46	

MECHANICAL STRESS DURING COLLISION

To determine whether local collision force predicts local mechanical stress, a regression analysis between contact force predictions and mechanical stress predictions is performed. For each time point during vocal fold collision and at each 1 mm interval along the vocal fold edge, contact force and medial superficial stresses are extracted from model results. Compressive stress perpendicular to the plane of contact, shear stress parallel to the plane of contact in the longitudinal direction, shear stress parallel to the plane of contact in the vertical direction, and Von Mises stress are examined. The relationship between contact force and stresses for a subglottal pressure of 1 kPa is dependent on the stress direction (Figure 2.6). At this subglottal pressure there is a general trend between increases in local contact force and increases in compressive stress (r^2=0.79), vertical shear stress (r^2=0.69) and Von Mises stress (r^2=0.83). There is no trend between local contact force and longitudinal shear stress (r^2=0.00).

Local variations from the general trends can be appreciated by examining the data points for each 1mm segment. The variations are most pronounced for longitudinal shear stress,

where there are local inverse trends between contact force and stress despite the lack of a general trend.

DISCUSSION

This model examines the time and spatial course of vocal fold closure, but not separation, during phonation and makes two contributions. The first contribution is reasonably accurate prediction of closure kinematics and collision surface forces, despite the absence of an aerodynamic representation and an assumption of homogeneous material properties. This provides insight as to the importance of elastic forces in glottal closure and supports future application to the study of the effects of vocal fold tissue elasticity and structure on the dynamics of glottal closure, corresponding aerodynamic variables and, by extension, voice quality.

The second contribution is an illustration of the potential of this model of glottal closure to provide a window to mechanical conditions in the vocal fold interior that may increase injury risk. Regressions between surface contact force and relative predictions of mechanical stress in the tissue indicate that the implications of experimental impact force measurements are position dependent and identify compressive stress perpendicular to the contact plane, shear stress parallel to the contact plane in the longitudinal direction and Von Mises stress as candidate mechanical stresses that may cause tissue damage as a result of high collision forces.

The ability of this model to predict closure kinematics and collision surface forces despite exclusion of aerodynamic forces from the model provides insight into the mechanics of voice production. Agreements between model predictions and published data suggest

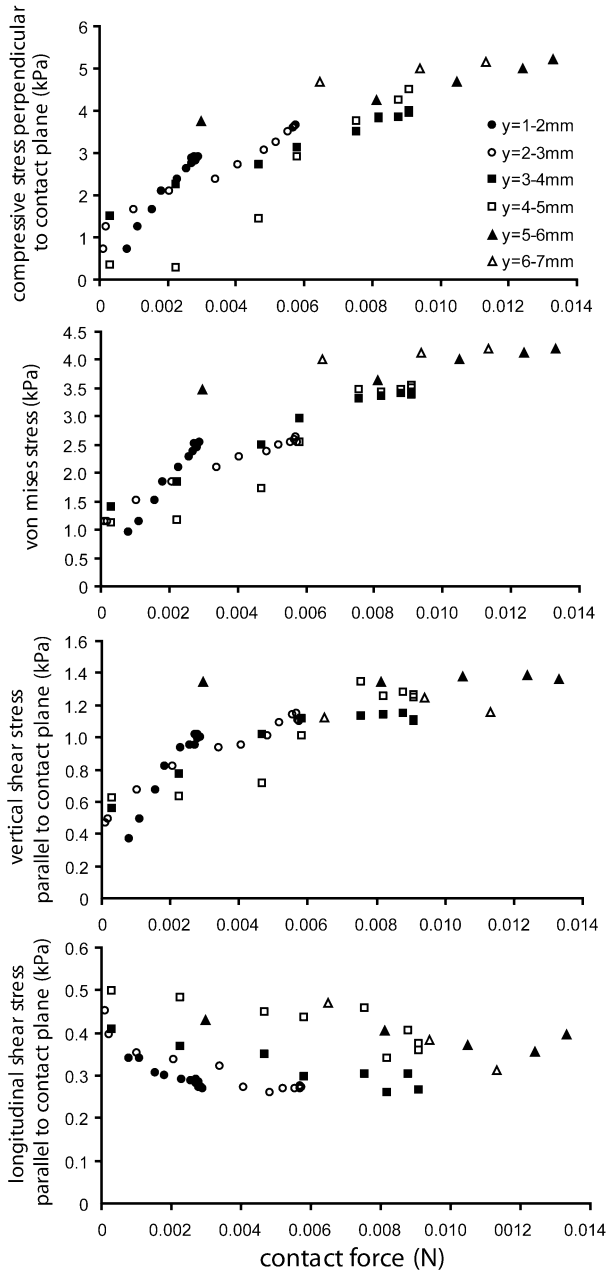

Figure 2.6: Relationship between local contact force and mechanical stress on the medial vocal fold surface during collision as predicted using a finite element model
The *x* value of each data point represents the integrated contact force over a 1mm vertical slice of the medial surface. The *y* value of each data point represents the maximum mechanical stress in the surface tissue in the same 1mm slice. Data is symmetric about the mid-membranous location ($y = 7$ mm). For simplicity only data for the anterior half of the fold are shown. Correlation coefficients are given in the text.

that elastic forces within the tissue dominate the mechanics of vocal fold closure and collision, and are therefore a major determinant of aerodynamic variables that are associated with closure, such as minimum flow and maximum flow declination rate (MFDR). The dependence of voice quality on MFDR and minimum flow allows extension of this hypothesis to propose that solid mechanics of vocal fold tissue are a dominant factor in voice quality. In vivo associations between structural changes that affect vocal fold closure, such as vocal nodules, increased minimum flow, decreased MFDR, and altered voice quality perceptions (Kuo, 1998) support this hypothesis.

The suggestion that tissue mechanics dominate vocal fold closure kinematics, important aerodynamic variables, and voice quality reinforces the proposed use of a vocal fold collision model to predict surgical outcomes. Comparison of the closure dynamics between models of vocal folds with organic pathologies and models of the same folds following surgical repair will allow prediction of the effects of surgery on voice quality. The prognostic value of this application may be further refined by incorporation of a layered geometrical structure and more complex material property definitions; these will facilitate the creation of higher fidelity models of pathology and surgical changes. This idea is explored in Chapter 4.

The lack of a defined contact force peak in models with low subglottal pressures and the lack of a reopening phase in all models does not agree with clinical observations of glottal opening, but was not an intended focus of this model. These results indicate that bouncing of the vocal folds following collision is not sufficient to cause glottal opening for the subglottal pressures and configurations studied and reinforces the important role played by air pressure in vocal fold separation. Comparison of the current results with

those from a new model with a sophisticated aerodynamic representation will test the hypothesis that tissue elasticity forces dominate during glottal closure and that aerodynamic forces dominate during vocal fold separation.

Agreement between model glottal closure kinematics and collision surface forces and experimental measurements does not necessarily imply that model predictions of mechanical stress are accurate. It is the case in any complex model with multiple input variables, that there may not be one unique combination that produces the desired output. In the case of this model, prediction of appropriate contact surface forces and closure kinematics only implies that one appropriate set of input parameters was identified. A different combination of input parameters may have provided the same surface contact force predictions, but different absolute mechanical stress predictions. However, it is likely that the relative nature of mechanical stress predictions would remain the same. Therefore it is reasonable to compare them against each other.

The relationships between contact forces on the vocal fold surface and superficial tissue mechanical stress in the medial edge of the vocal fold, derived using a model of vocal fold collision, guide the interpretation of experimental contact force measurements, such as those presented in Chapter 5. Local collision force measurements are indicative of local compressive stress, vertical shear stress, and Von Mises stress. This observation suggests that pathologies associated with maneuvers that have increased local impact forces (e.g. phonation with high subglottal pressures) may be due to a compressive mode of tissue failure, a shear mode of tissue failure or alterations in cellular behavior. Unfortunately, without knowledge of what stress magnitudes cause tissue failure, it is impossible to comment on which stress levels are most damaging to the tissue.

Correlations between stress predictions and epidemiology of lesions that reflect tissue injury, such as vocal nodules, will test the impact stress hypothesis of pathology development. This is explored in Chapter 3.

Additional experimental measurements will improve definition and validation of the vocal fold collision model and other models of vocal fold tissue mechanics. Three dimensional material property data based on human vocal fold tissue samples undergoing compression would improve the fidelity of model inputs. In vivo human results of surface collision forces would be a preferred source against which to validate model predictions because agreement will enhance the applicability of the model to human voice. Such measurements are presented in Chapter 5. Other experimental measurements that will be useful in validation include electoglottographic measurements of contact area and photoglottographic measurements of glottal area.

CHAPTER 3: MODELING MECHANICAL STRESSES AS A FACTOR IN THE ETIOLOGY OF BENIGN VOCAL FOLD LESIONS[1,2]

INTRODUCTION

Vocal nodules and polyps are convex lesions on the midline of the medial surface of the vocal folds associated with excessive voice use, loud voicing, inadequate hydration, and voice misuse (Buckmire and Rosen, 2001). Mechanical stress during vocal fold collision is implicated as a cause of benign vocal lesions, such as vocal nodules and vocal polyps, based on observations of high velocity impact between vocal folds during speech (Titze, 1994) and of structural disruptions of the basement membrane in these lesions (Gray and Titze, 1988). Experimental investigation of this hypothesis is impeded by the difficulty of quantifying spatial and temporal stress variations in the small tissue volume (1-2 cm^3) that vibrates, on average, between 100 and 200 Hz during voice production and the challenge of measuring and manipulating independent variables such as tissue stiffness.

[1] Portions of this work were presented in "Mechanical stress levels in vocal folds as predictors of tissue injury" International Conference on Voice Physiology and Biomechanics, Denver, CO, September 17-19, 2002.

[2] This work has been submitted for publication as Gunter, H.E. (2003) "Modeling Mechanical Stresses as a Factor in the Etiology of Benign Vocal Fold Lesions" to the Journal of Biomechanics (JB2002-187)

Theoretical models of vocal fold tissue mechanics are an ideal alternative research platform since they can predict spatial and temporal stress variations at appropriate resolutions and permit manipulation and control of geometric and material parameters that may influence these variations.

This chapter presents new computational models and their application to investigating the hypothesis that vocal fold tissue lesions such as nodules and polyps develop in response to mechanical stress occurring during vocal fold collision. A one-dimensional lumped mass model illustrates the concept of mechanical stress during collision and predicts the influence of material and geometric parameters on compressive stress magnitude. A three-dimensional finite element model of vocal fold collision with temporal resolution that captures the dynamics of collision and spatial resolution smaller than that of tissue pathology (discussed in chapter 2) predicts spatial variations of stress tensor components. Model predictions are evaluated within the framework of the epidemiology of benign changes in vocal fold structure such as nodules and polyps. Improved understanding of the proposed mechanical etiology of these lesions has implications for their prevention and treatment in the clinic.

METHODS

Lumped mass model

A simple spring mass model (Figure 3.1c), inspired by the lumped mass models of vocal fold movement that have been useful in the speech synthesis domain (for example, (Ishizaka and Flanagan, 1972)) generates an approximation for superficial normal stress in vocal fold tissue during collision with the opposing fold. The model approximates a coronal vocal fold cross section (Figure 3.1a) as two layers: a cover composed of the

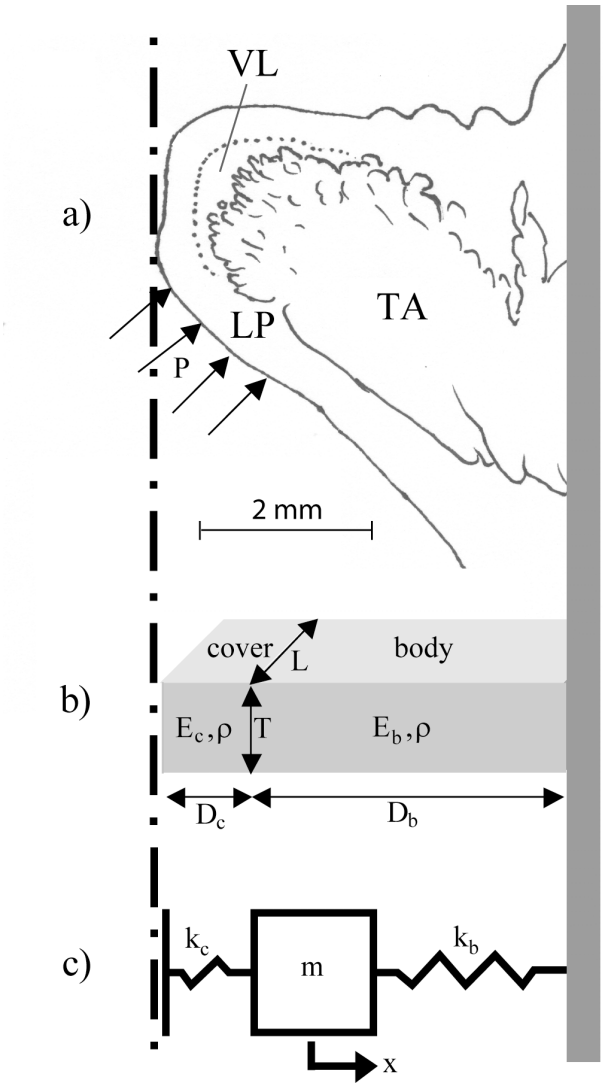

Figure 3.1: Development of a lumped mass model of vocal fold collision.
The dashed line indicates the plane of collision between opposing vocal folds in the center of the larynx. The gray line on the right represents the fixed boundary formed by the laryngeal cartilages. **(a)** Sketch of a histological cross section illustrating the layered structure of the vocal fold - LP: lamina propria, VL: vocal ligament, TM: thyroarytenoid muscle. The arrows indicate the direction that air pressure acts during voice production **(b)** Rectangular prism representation of a vocal fold with two layers that serves as a conceptual intermediate between the anatomical structure in (a) and the lumped mass model in (c). Cover represents the mucosa and ligament. Body represents the muscle. Each layer is defined by geometric properties of depth (D), thickness (T) and length (L) and material properties density (ρ) and stiffness (E). Nominal values of all parameters are given in Table 1. **(c)** One-dimensional lumped mass representation of a vocal fold defined by 3 parameters (m, k_c, k_b) that are defined by rectangular prism model parameters.

mucosa and underlying connective tissue, and a body composed of the thyroarytenoid muscle. Springs (k_c, k_b) in series define the two layers and a mass (m) at the junction of the springs represents the center of gravity. Interaction with the opposing fold occurs through the cover spring (k_c): When the folds are separated ($x > 0$), this spring is not deformed. When the folds are in contact ($x < 0$), the cover spring is constrained by the opposing fold at the midline plane, and deforms accordingly.

Closure of the glottis begins when the vocal folds are maximally separated. In this configuration the cover spring is not constrained and the system is described by a second order differential equation, which is valid until the folds are in contact.

$$m\ddot{x} + k_b x = 0 \quad valid\ for\ x \geq 0 \tag{3.1}$$

x is the lateral displacement of the vocal fold away from its neutral position. For a maximum opening equal to x_o and an initial velocity of zero, the pre-collision solution for movement of the vocal fold is valid from the time of release until $x = 0$.

$$x = x_0 \cos\left(\sqrt{\frac{k_b}{m}}t\right) \quad for\ 0 \leq t \leq \frac{\pi}{2}\sqrt{\frac{m}{k_b}} \tag{3.2}$$

When the center of gravity crosses its neutral position the cover spring becomes constrained by contact with the opposing fold at the midline plane and begins to deform. The system is now described by another second order differential equation, which is valid until $x > 0$, when the folds cease to be in contact.

$$m\ddot{x} + (k_c + k_b)x = 0 \quad valid\ for\ x \leq 0 \tag{3.3}$$

Using initial conditions for position and velocity from the boundary of the precollision solution (equation 3.2), the postcollision solution is obtained.

$$x = -x_0\sqrt{\frac{k_b}{k_c+k_b}}\sin\left[\sqrt{\frac{k_c+k_b}{m}}\left(t-\frac{\pi}{2}\sqrt{\frac{m}{k_b}}\right)\right] \quad for \quad \frac{\pi}{2}\sqrt{\frac{m}{k_b}}t \le \frac{\pi}{2}\left(\sqrt{\frac{m}{k_b}}+2\sqrt{\frac{m}{k_c+k_b}}\right) \tag{3.4}$$

The frequency of vibration (F_0) is the inverse of the average of the pre- and post-collision periods.

$$F_0 = \pi^{-1}\left(\sqrt{\frac{m}{k_c+k_b}}+\sqrt{\frac{m}{k_b}}\right)^{-1} \tag{3.5}$$

Stress in superficial tissue is the product of the spring constant (k_c) and the displacement of the mass (x) divided by a cross sectional area (A). For noncollision phases ($x > 0$) stress is equal to zero since the cover spring is not deformed. For collision phases stress is a function of the location of the mass (equation 3.4).

$$\sigma_{xx} = -\frac{k_c x_0}{A}\sqrt{\frac{k_b}{k_c+k_b}}\sin\left[\sqrt{\frac{k_c+k_b}{m}}\left(t-\frac{\pi}{2}\sqrt{\frac{m}{k_b}}\right)\right] \tag{3.6}$$

The lumped mass parameters are expressed in terms of physiological variables by comparing them to a rectangular prism approximation of a vocal fold (Figure 3.1b) that is defined by geometric and material parameters from the literature (Table 3.1). Consideration of longitudinal compression of the beam generates expressions for lumped mass parameters in terms of material and geometric properties of the beam (Table 3.2). The maximum compressive stress during collision in terms of physiological variables is

obtained by substituting the expressions relating physiological and lumped mass variables (Table 3.2) into the amplitude of the stress expression (equation 3.6).

Table 3.1: Typical vocal fold dimensions and material properties from the literature

Parameter	Symbol	Nominal Value	Source
Length	L	1.5 cm	Hirano et al, 1988
Thickness	T	0.25cm	Perlman & Durham, 1987
Cover depth	D_c	0.11cm	Hirano et al, 1983
Body Depth	D_b	1cm	Tayama et al, 2002
Cover Stiffness	E_c	36.1kPa	Min et al, 1995
Body Stiffness	E_b	20.7kPa	Alipour-Haghighi & Titze, 1991
Tissue density	ρ	$1.0 g/cm^3$	
Driving Pressure	P	0.8 kPa	

Table 3.2: Lumped model parameters in terms of biomechanical variables

Parameter	Relationship
A	LT
M	$LT(D_c+D_b)\rho$
k_c	E_cLT/D_c
k_b	E_bLT/D_b
X_0	PD_b/E_b

$$\sigma_{xx\max} = -\frac{PE_cD_b}{D_cE_b}\sqrt{\frac{\frac{E_b}{D_b}}{\frac{E_c}{D_c}+\frac{E_b}{D_b}}} \tag{3.7}$$

P is the air pressure that maximally separates the vocal folds. E_c and E_b are the Young's moduli of the cover and body layers. D_c and D_b are the depths of the cover and body layers. Frequency of vibration in terms of physiological variables is obtained by substituting the biomechanical expressions (Table 3.2) into the frequency equation (equation 3.5),

$$F_0 = \pi^{-1}\left[\sqrt{\frac{\rho(D_c + D_b)}{\frac{E_c}{D_c} + \frac{E_b}{D_b}}} + \sqrt{\frac{D_b^2}{E_b}}\right]^{-1} \tag{3.8}$$

where ρ is the density of the tissue. Predictions made using these equations provide insights into the variables contributing to superficial stress in vocal fold tissue during vocal fold collision and are directly comparable with predictions made using a more complex model.

Finite element model

A three-dimensional model of vocal fold closure and collision, implemented using commercial finite element software (Abaqus Standard 5.8-1, Abaqus Inc., Pawtucket, RI), generates spatial and temporal predictions of the stress tensor. The model consists of 14,242 ten noded tetrahedral linear elastic elements that define a single vocal fold (Figure 3.2a). This number of elements provides a resolution of 250 μm, which is necessary to examine the formation of 500 μm pathologies such as vocal nodules. The geometric arrangement of the elements is based on human male vocal fold dimensions used by Titze and Talkin (1979). Their material properties (E=36.1 kPa, ν=0.3) are based on human vocal fold ligament measurements made by Min, et al. (1995) that have been used in previous finite element models of vocal fold tissue (Jiang et al., 1998). The assumption of isotropy is made due to lack of quantitative data to guide statements of anisotropy. The assumption of elasticity is based on evidence that viscous properties of vocal fold tissue make negligible contributions to deformations at voicing frequencies (i.e. damping ratio of 0.01 at 100 Hz) (Chan and Titze, 2000).

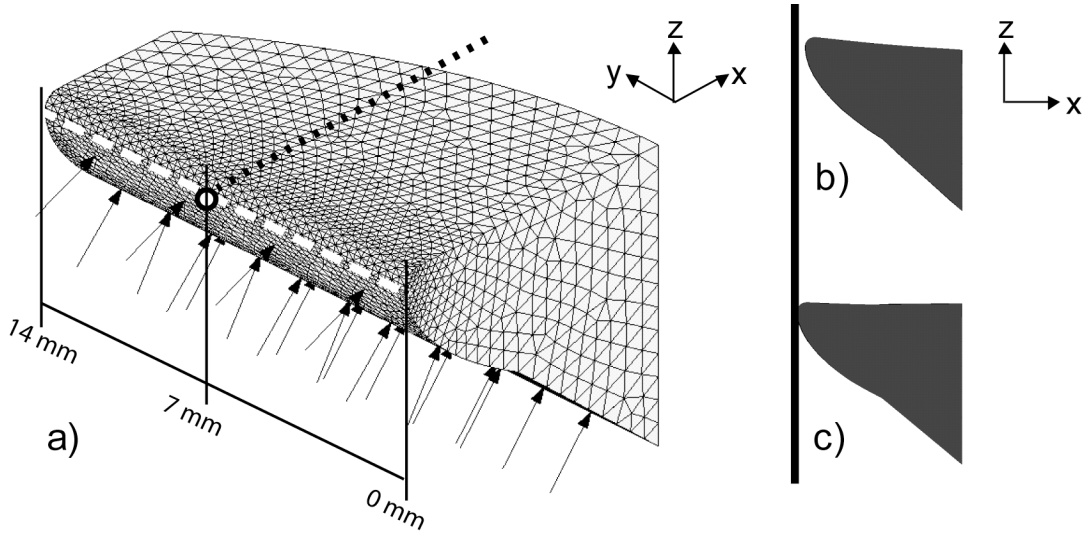

Figure 3.2: Finite element model of vocal fold collision
(a) Three-dimensional geometric structure based on measurements of human vocal folds. Divisions indicate the boundaries of elements. Each element is defined by material properties taken from the literature. Arrows indicate driving pressure load. Dashed white line follows vocal fold edge, along which stresses are examined. Numbers indicate reference points for locations on the vocal fold edge. White circle indicates injury prone region at the center of the vocal fold edge. Dashed dark line indicates section cut for right hand images. **(b)** Cross-section showing initial condition for vocal fold collision model (t = 0 s). Deformation is the static solution to the driving pressure load. Solid black line indicates the collision plane. **(c)** Cross-section of dynamic vocal fold collision model at t = 0.2 s illustrating collision between the medial vocal fold surface and the collision plane.

The model predicts tissue deformation of and forces in vocal fold tissue during a single vocal fold closure. It does not include a representation of the airflow between the vocal folds. This simplification is suggested by data indicating that air pressures between the vocal folds are low during glottal closure and vocal fold collision (Alipour et al., 2001) and is supported by the ability of this model to generate reasonably accurate predictions of vocal fold closure dynamics and collision kinematics (Chapter 2). The initial condition for vocal fold closure is the static solution for deformation by a medial driving pressure (P) (Figure 3.2b). The solution for vocal fold closure is the transient dynamic recoil of the unloaded vocal fold from this initial configuration. Collision with the opposing fold is defined by a collision pairing between a rigid midline plane and nodes on the medial surface of the vocal fold. This reflects an assumption of left-right symmetry in the larynx. The solution includes movement of the tissue towards its neutral position and collision with a midline plane (Figure 3.2c) and is calculated using an implicit integration algorithm with automatic time incrementation and consideration of geometric nonlinearities. Details of model development, calculation of a natural frequency of 128 Hz, and validation against experimental measurements of collision forces in excised larynges are discussed elsewhere (Chapter 2). The magnitude of the driving pressure in the finite element model is manipulated in a range that is typical of human voice production (0.4 kPa to 1.4 kPa). For each pressure the three normal stresses (σ_{xx}, σ_{yy}, σ_{zz}) and the three shear stresses (σ_{xy}, σ_{yz}, σ_{zx}) are examined spatially and temporally.

Values that characterize regional stress magnitudes are used to compare post-collision stresses. Regions are defined by a node along the vocal fold edge and seven elements

within ± 0.125 mm of that node. The composite stress waveforms are averages of the centroidal stresses in each element at each time point. The characteristic post-collision stress for a region is the maximum composite stress magnitude that occurs during the post-collision period, which is 0.25 ms in duration and begins when the node at the center of the region contacts the collision plane. This duration constraint reflects the start of the opening phase of vocal fold vibration, which this model does not represent. Post-collision characteristic stresses are calculated for each driving pressure at seven regions spaced 2 mm apart along the vocal fold edge.

RESULTS

The closed form nature of the lumped mass model of vocal fold collision facilitates a comprehensive analysis of the effects of independent variables. The predicted frequency is 115 Hz. The predicted peak superficial compressive normal stress ($-\sigma_{xx}$) is 3.1 kPa. According to this model, stress is independent of vocal fold length and thickness, is linearly related to driving pressure, correlates positively with increases in muscle depth, and cover stiffness, and correlates negatively with increases in muscle stiffness, and cover depth (Figure 3.3a,b). Frequency is increased by increases in either muscle stiffness or cover stiffness (Figure 3.3c). The relationship between normal stress and frequency is direct if cover stiffness is manipulated and inverse if muscle stiffness is manipulated to create the change in frequency (Figure 3.3d). These results are summarized in Table 3.3.

The finite element model permits three-dimensional examination of the entire stress tensor. There are increases in the magnitude of all compressive normal stresses (σ_{xx}, σ_{yy},

$\sigma_{zz} < 0$) and vertical shear stress on the plane tangent to the vocal fold edge (σ_{xz}) following collision in an element in the injury prone region for a driving pressure of 0.8 kPa (Figure 3.4). These trends are typical of all superficial elements along the vocal fold edge. There is no discernible relationship between collision and the remaining shear stresses (σ_{xy}, σ_{yz}) or tensile stresses (σ_{xx}, σ_{yy}, $\sigma_{zz} > 0$).

Table 3.3: Effect of physiological parameter manipulation on compressive stress magnitude as predicted by a lumped mass model of vocal fold collision

Physiological parameter manipulated	change in compressive stress magnitude
Volume differences	
↑ driving pressure	↑
Anatomical differences	
↑ muscle depth	↑
↑ cover depth	↓
Implementation differences	
↑ frequency by ↑ muscle stiffness	↓
↑ frequency by ↑ cover stiffness	↑

The spatial and driving force effects on characteristic stresses are investigated for stresses that are influenced by collision. All compressive stresses and the vertical shear stress on the collision plane are elevated in the injury prone area (i.e. distance from the anterior boundary = 7 mm) for a driving pressure of 0.8 kPa (Figure 3.5). The collision plane ($-\sigma_{xx}$) and vertical ($-\sigma_{zz}$) compressive normal stress maxima at the injury prone region are global maxima for the model. The horizontal compressive normal ($-\sigma_{yy}$) and vertical collision plane shear (σ_{xz}) have higher values on the anterior vocal fold boundary during the pre-collision period. Increased driving pressure increases post-collision stress magnitudes at the injury prone region (Figure 3.6). All compressive stresses are linearly related to driving pressure ($r^2 > 0.9$).

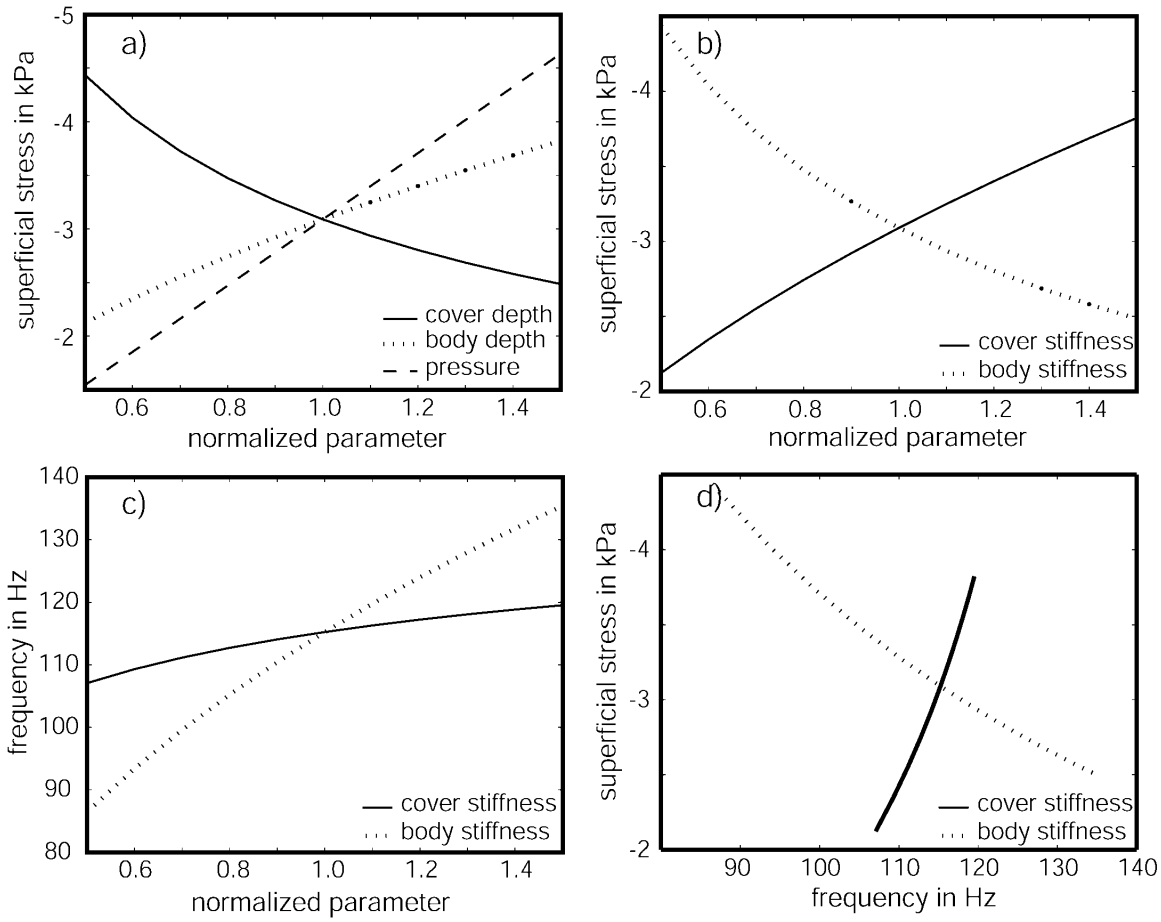

Figure 3.3: Dependence of superficial stress in vocal fold tissue during collision and vocal fold vibration frequency (i.e. pitch) on geometric and material parameters as predicted by a lumped mass model of vocal fold collision.
Each curve is generated by manipulating a single parameter while maintaining all others at their nominal value. Negative stresses are compressive. Stress axes are reversed to illustrate compressive stresses. All manipulated parameters are normalized to the nominal values given in Table 3.1.

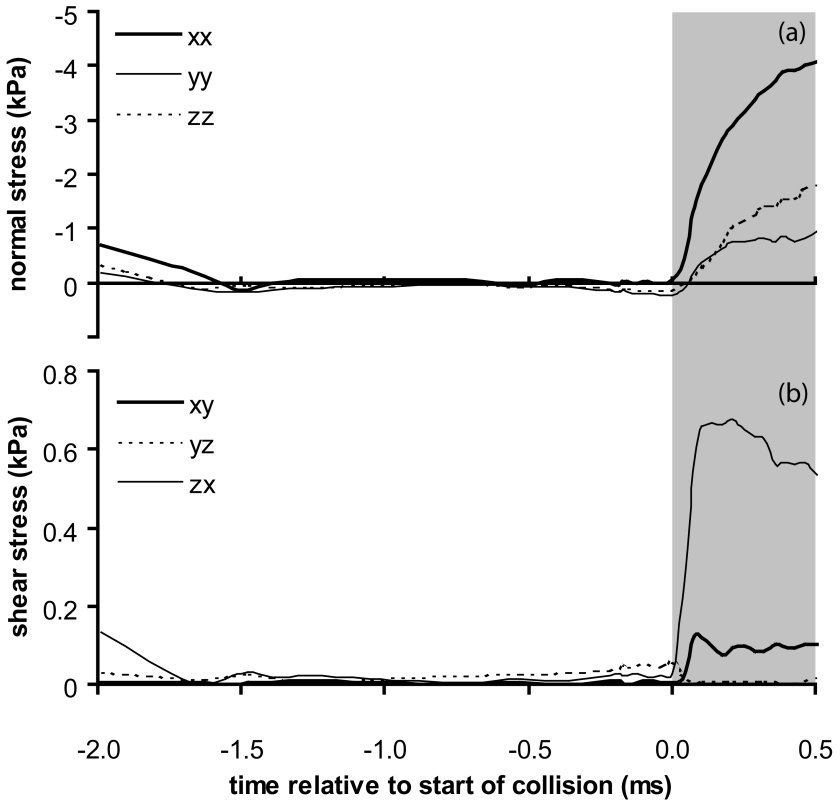

Figure 3.4: Effect of vocal fold collision on components of the stress tensor at the injury prone region for a driving pressure of 0.8 kPa as predicted with a finite element model. Time = 0 is the beginning of collision. Shaded area indicates post collision period **(a)** Normal stresses during vocal fold closure and collision. Tensile stresses are greater than zero. Compressive stresses are less than zero. Stress axis is reversed to illustrate compressive stress magnitudes. **(b)** Shear stresses during vocal fold closure and collision.

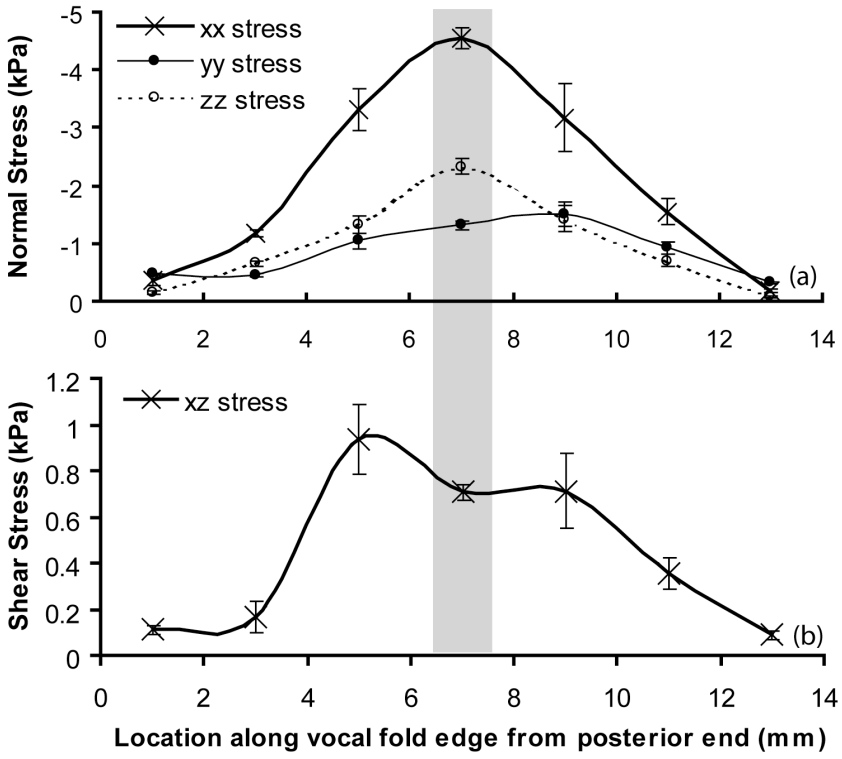

Figure 3.5: Spatial variation of stress tensor components in superficial tissue along the vocal fold edge for a driving pressure of 0.8 kPa as predicted by a finite element model. Shaded area is the injury prone region. Each point is a spatial average of 7 elements. Error bars are standard error for the 7 elements that indicate the extent of spatial variation of stresses. **(a)** Normal stresses along vocal fold edge during collision. Negative stresses are compressive. Stress axis is reversed to illustrate compressive stresses. **(b)** Shear stress in the vertical direction on a plane parallel to the collision plane. Asymmetry reflects geometric asymmetry of the model.

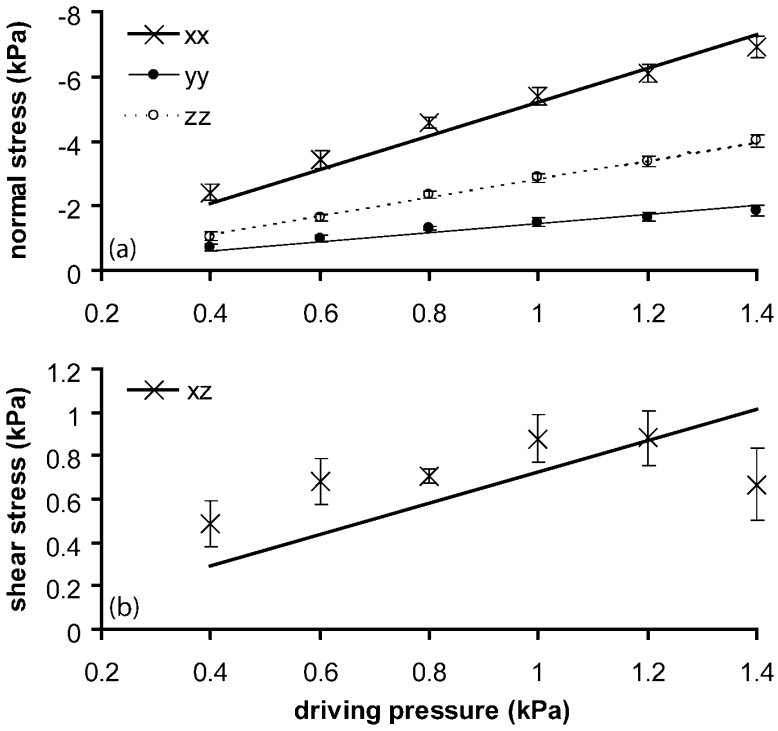

Figure 3.6: Dependence of stress tensor components in the injury prone region during collision on driving pressure as predicted by a finite element model.
Each point is a spatial average of 7 elements. Error bars are standard error. Lines are fit using the method of least mean squares. **(a)** Relationship between driving pressure and compressive stress magnitudes. Curves are based on linear regression analysis. Stress axis has been reversed to illustrate compressive stresses. **(b)** Relationship between driving pressure and shear stress in the vertical direction on a plane parallel to the collision plane. Curve is based on linear regression analysis

DISCUSSION

Two computational models, one simple and one complex, provide estimations of mechanical stress in vocal fold tissue during vocal fold collision in order to investigate the role of stresses as a cause of tissue injuries that lead to the developments of lesions such as nodules and polyps. A one-dimensional lumped-mass model (Figure 3.1c) parameterizes vocal fold tissue mechanics to generate closed form solutions. Predictions are limited to superficial compressive normal stress perpendicular to the plane of collision ($-\sigma_{xx}$) during vocal fold collision. A three-dimensional finite element model (Figure 3.2) assumes isotropic linear elasticity, material homogeneity and simplified aerodynamics to generate numerical solutions of the stress tensor. Predictions of stress tensor components are limited to the closing phase of vocal fold vibration including collision between the vocal folds as represented by collision between a single vocal fold and a rigid plane.

The predictions of the finite element model and lumped mass model agree with published theoretical and experimental data. The frequencies predicted by both models fall within the normal range of human male voice (Zemlin, 1997). The suggestion made by the lumped mass model that increases in cover and body stiffness increase frequency (Figure 3.3c) is consistent with in vivo EMG measurements by Shipp and McGlone (1971) and stiffness measurements by Berke and Gerratt (1993), which indicate that activity in the thyroarytenoid muscle that composes the body increases vocal fold stiffness and pitch and that activity in the cricothyroid muscle, which longitudinally lengthens the hyperelastic vocal fold cover, also increases stiffness and pitch. However, independent manipulation of body and cover stiffnesses is not consistent with voice physiology since

activity in the thyroarytenoid muscle also longitudinally shortens the hyperelastic vocal fold cover and therefore causes a decrease in effective cover stiffness in addition to an increase in body stiffness. The linear relation between driving pressure and collision stress, which is proportional to collision force, in the lumped-mass model is consistent with the experimental observations of Jiang and Titze (1994) and earlier predictions made using the finite element model (Chapter 2). Predictions of compressive stress during collision by the lumped mass model are the same order of magnitude as those made with the finite element model (Chapter 2).

Predictions made by the finite element model support and expand the hypothesis that benign vocal fold pathologies such as nodules and polyps are a reaction to mechanical stress. The magnitudes of multiple components of the stress tensor increase during collision in the region where pathologies often develop (i.e. center of the vocal fold edge)(Figure 3.5). This is also the region that attains the highest velocity immediately prior to contact. Therefore the stresses reflect the development of elastic energy as contact forces decelerate the tissue. The nature of the increased components suggests possible mechanisms of tissue damage that lead to lesions, such as nodules and polyps, which are characterized by basement membrane disruption (Gray and Titze, 1988) and expanded extracellular matrix (Mossallam et al., 1986). The collision-associated compressive stress maxima in two coordinate directions and elevated compressive stress in the third at the injury prone region (Figure 3.5a) are of similar magnitude to those that increase protein synthesis and secretion by tracheal epithelial cells in culture as shown by Swartz et al. (2001) and are therefore likely to lead to an expansion of the extra-cellular matrix. Vertical shear stress on the plane parallel to collision is elevated at the injury

prone location (Figure 3.5b) and is of the appropriate orientation to cause the disrupted adhesions between epithelial cells and the basement membrane. The lack of tensile stress in the injury prone region during collision (Figure 3.4a) suggests that tension is not the cause of tissue failure that leads to vocal nodule and polyp formation. In the absence of data pertaining to the dose response of vocal fold tissue elements to the components of the stress tensor it is difficult to say which magnitudes and directions of stress pose the greatest injury risks. Carefully controlled studies using vocal fold tissue culture models would further guide interpretation of these results. Such models would also permit study of the role played by frequency of deformation in tissue injury.

The models provide insights into mechanical bases for risk factors associated with development of vocal fold pathologies. Sound intensity varies with driving pressure (Isshiki, 1964). Therefore, the linear relationship between driving pressure and compressive stress magnitude in the region that is prone to injury (Figure 3.6a) provides an explanation for the presumed association between high volume voicing and formation of pathologies. The inverse contribution of cover depth to compressive stress magnitude (Figure 3.3a) offers an explanation for proposed protective nature of hydration and warm up against vocal fold injury since both are likely to increase fluid volume in, and depth of, the cover. The prediction by the lumped mass model that mechanical stress is dependent on the method of frequency manipulation (Figure 3.3d) addresses the role played by voicing practice in determining mechanical stress levels and risk of tissue injury. According to these predictions, it is conceivable that two individuals with similar anatomy may produce sounds of similar pitch and volume using different production strategies (i.e. different muscle activation patterns) and therefore have different

mechanical stress levels and injury risk. This lends credibility to anecdotal evidence that lack of training or inappropriate training leads to voice "misuse" and increased risk of lesion formation. It also suggests that information on how voice is generated may prove useful for clinical diagnosis and treatment of these benign lesions.

The results of the models discussed in this paper provide inspiration for additional models of vocal fold tissue. Each model was used for its relative strengths; the lumped mass model facilitated parameter sensitivity studies, and the finite element model facilitated physiological fidelity. Additional simple models that address stresses other than compressive stress in the direction perpendicular to the plane of collision would permit further parameter variation studies. Finite element models that incorporate a broader spectrum of input variables with increased complexity (for example, isotropic nonlinear viscoelasticity and material inhomogeneity) would provide further validation of the simple models. Models of both types would be useful for addressing sources of vocal fold tissue stress other than collision, for example those induced by changes in laryngeal configurations. Inhomogeneous finite element models are presented in Chapter 4.

CHAPTER 4: A THEORETICAL INVESTIGATION OF THE ROLE OF SUPERFICIAL LAMINA PROPRIA STIFFNESS DURING VOICE PRODUCTION[1]

INTRODUCTION

The superficial lamina propria (SLP) is a soft connective tissue matrix containing elastin and collagen fibers that lies beneath the epithelia of the vocal folds and of other surfaces in the human body. It is implicated as an important contributor to the mechanics of voice production (Gray et al., 2000). Pathological changes to SLP structure such as scar are associated with deteriorating voice quality (Cotron and Casper, 1996) and surgical augmentation is reported to restore voice quality (Zeitels et al., 2002). Its viscous properties are linked with phonation threshold pressure (Titze et al., 1995) and its deformation contributes to a mucosal wave on the superior vocal fold surface (Berke and Gerratt, 1993), qualitative assessment of which is part of a clinical voice evaluation. Quantitative understanding of the relationship between SLP stiffness and movement of

[1] This work has been submitted for publication as Gunter, H.E. (2003) "Theoretical investigation of the role of superficial lamina propria stiffness during voice production" to the Journal of the Acoustical Society of America

the vocal folds has applications in surgical planning and tissue engineering of replacement SLP.

The contributions of the soft elastic properties of the SLP to voice mechanics have received little quantitative attention. Rheometric data confirm anecdotal reports that the superficial lamina propria has important viscous properties at low deformation frequencies ($\xi = 0.1 - 1$) and is over 100 fold less stiff for incremental strains from rest length than other vocal fold tissues (Chan and Titze, 1999a). Some theoretical models of vocal fold tissue purport to represent the SLP by including it in a vocal fold cover layer that is defined using data collected from samples including both epithelium and SLP in parallel undergoing longitudinal tension (Alipour et al., 2000;Jiang et al., 1998). This is not a good representation of the SLP behavior since, at low strain rates, properties of the relatively nonviscous and stiffer epithelium dominate such data (Alipour-Haghighi and Titze, 1991;Kakita et al., 1981). More accurate quantification of the SLP's material properties is challenging due to its frequency dependent behavior. The behavior of epithelium and SLP samples in series undergoing dynamic transverse shear deformations provide an indication of the viscoelastic properties of the SLP in the frequency range that the rheometer operates in (Chan and Titze, 1999a). Theoretical extrapolations of this data to deformation frequencies characteristic of voice predict that the SLP behaves in a predominantly elastic fashion ($\xi < 0.01$ for a human male sample) during voice production and remains much less stiff than other vocal fold tissues (Chan and Titze, 2000).

This chapter presents an investigation of the contributions of superficial lamina propria elasticity to voice mechanics including effects on collision force, tissue stress and glottal area dynamics. A finite element model that builds upon a previous model of vocal fold closure and collision (Chapter 2) by incorporating four tissue layers including distinct epithelium and superficial lamina propria layers is used.

METHODS

A finite element model of the vocal fold that represents four layers of tissue has been developed based on a single layer model of vocal fold closure and collision (Chapter 2). There are three differences between the current model and the previous model. The lateral contour of the vocal fold geometry is represented linearly rather than curvilinearly in the transverse plane. This geometric simplification has been implemented in other models with good results (Alipour et al., 2000). The geometry represents one half of a single vocal fold rather than an entire vocal fold. This reflects recognition of anterior-posterior symmetry that is created though the use of a linear lateral boundary and reduces computational time by a factor of two. The vocal fold geometry is subdivided into four layers with distinct material definitions rather than being defined homogeneously using one material definition.

The external and internal dimensions of the hemi-fold model are based on histological section measurements. The midmembranous to end length is 7 mm and the vocal fold depth and height are both 10 mm (Figure 4.1). These external dimensions have been used in previous models (Alipour et al., 2000;Gunter, 2003a, b;Titze and Talkin, 1979). The dimensions of the four layers that define the vocal fold cross section are based on

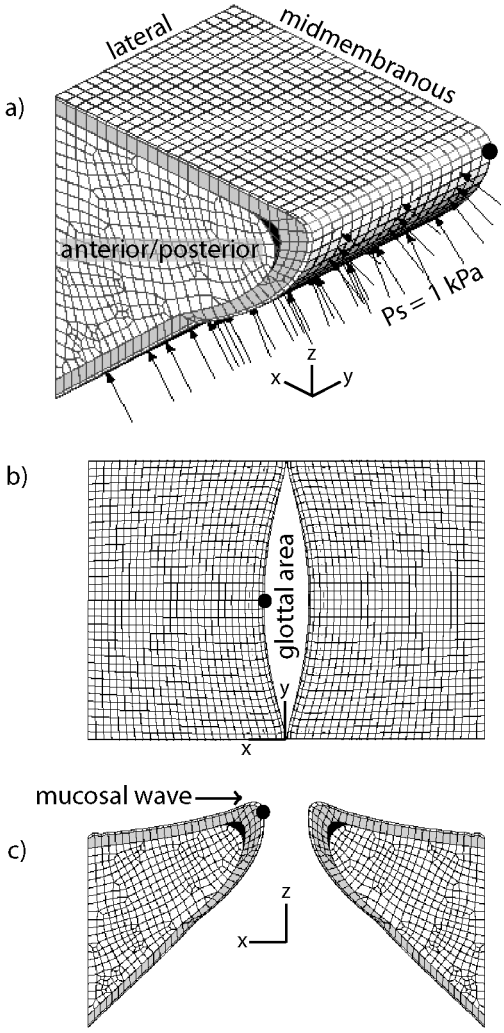

Figure 4.1: Finite element model of vocal fold closure and collision with four distinct tissue layers.
(a) Three dimensional structure representing half of a single vocal fold. White elements on the model exterior represent the epithelium, gray elements represent the SLP, black elements represent the ligament and white elements on the model interior represent the thyroarytenoid muscle. Each material has distinct isotropic elastic properties. The lateral and anterior / posterior surfaces are fixed in three dimensions and the midmembranous surface is fixed only in the y dimension. The arrows indicate the application of a 1 kPa pressure that is used to calculate the initial condition for the closure process. The black circle indicates the medial midmembranous location where stresses and strains are examined.**(b)** Superior view of a time point during glottal closure. The results of the half model are reflected to illustrate the entire glottis. The two dimensional space between the vocal folds is the glottal area. The black circle indicates the midmembranous location where stresses and strains are examined. **(c)** Coronal section at the midmembranous surface of the half vocal fold model at the same time point of glottal closure shown in panel b. The results of the half vocal fold model are reflected in order to illustrate the opposing fold. The upturned portion of the vocal fold edge is the crest that initiates the mucosal wave. The element colors indicate the tissue layers (see a).

data from human vocal folds (Hirano et al., 1983). The 0.1 mm thick epithelium and 0.6 mm thick SLP form the medial and superior surfaces of the vocal fold. The 0.2 mm thick ligament is located in the vocal fold apex, beneath the SLP. The muscle defines the interior of the vocal fold between the lateral boundary and the SLP and ligament (Figure 4.1). The tissues are defined with 9036 hexahedral (i.e. brick shaped) finite elements each defined with 20 nodes with three degrees of freedom. The lateral and end boundaries are fixed (i.e. are not permitted to translate) and the midmembranous boundary is fixed to its plane (i.e. it is permitted to slide along the plane). This latter boundary accounts for anterior/posterior symmetry of the vocal fold. The nodes on the medial boundary are free if their location is in the positive x domain, but are not permitted to translate into the negative x domain. This boundary definition effectively defines a contact plane at $x = 0$, which defines the midglottis.

Isotropic linear elastic material properties are assigned to each tissue layer (Table 4.1). The values defining the ligament and muscle are approximations (Min et al., 1995) based on the behavior of human ligament (Min et al., 1995) and canine muscle (Alipour-Haghighi and Titze, 1991) under longitudinal tension. The value defining the behavior of the epithelium is an approximation (Min et al., 1995) based on the behavior of canine mucosa (i.e. epithelium and superficial lamina propria) under longitudinal tension at low strain rates (Min et al., 1995). Since the epithelium and lamina propria are in parallel for longitudinal tension, the viscous lamina propria likely has minimal effect on the resistance of the sample to strain. Therefore this value is representative of the behavior of the epithelium. These linear approximations are valid for strains of 15% (Min et al., 1995), a limit that is not exceeded during model calculations. The values defining the

superficial lamina propria range from ten fold to two fold less stiff than the muscle. This range extends from the minimum linear stiffness necessary for model convergence to stiffness that is the same order of magnitude as the epithelium and is consistent with representations of the superficial lamina propria in other layered models (Alipour et al., 2000;Jiang et al., 1998). It is difficult to evaluate which if any of these values are physiologically relevant since there is no data on the large strain behavior of the superficial lamina at high frequencies, only data on low strain behavior at low frequencies (Chan and Titze, 2000). Isotropic definitions are used due to a lack of data to guide anisotropic material models. Poisson's ratios of 0.49 reflect near incompressibility of the tissues and are consistent with observations of other biological tissues.

Table 4.1: Material properties of vocal fold tissues used in a finite element model of vocal fold collision

Tissue	Young's Modulus (E) in kPa	Poisson's Ratio (ν)
Epithelium	41.9	0.49
Superficial Lamina Propria	2.0, 5.0, 10.0, 41.9	0.49
Ligament	36.1	0.49
Muscle	20.7	0.3

Movement of the tissue during vocal fold closure and collision is formulated as a dynamic contact problem. The initial condition for vocal fold closure is the static solution for deformation by a medial driving pressure (P), which is kept constant at 1 kPa in all models. The solution for vocal fold closure is the transient dynamic recoil of the unloaded vocal fold from this initial configuration and includes movement of the tissue towards its neutral position and collision with the midline plane. It is calculated using an implicit integration algorithm with automatic time incrementation and consideration of geometric nonlinearities. Both solutions are calculated using Abaqus 6.2-5 (Abaqus inc.,

Pawtucket, RI). Validation of this method against experimental and clinical data is described elsewhere (Chapter 2).

The results of four models that differ in the stiffness of the SLP are compared. The midmembranous contour of the vocal fold in a coronal plane at the initial condition for glottal closure provides a snapshot of the crest that becomes the mucosal wave (Figure 4.1c). Height of the mucosal wave crest is the vertical difference between the most superior point on the deformed vocal fold surface and linear extrapolation of the contour of the lateral half of the coronal section to the same point. Glottal area (i.e. the area between the vocal folds, denoted by A) is calculated by summing the areas of trapezoids formed by adjacent nodes on the vocal fold edge and the midline (Figure 4.1b). This quantity is used as an indicator of glottal air flow based on experimental data that illustrate a direct relationship between glottal area and flow if the pressure drop across the glottis (ΔP) is constant (Stevens, 1998):.

$$\Delta P \alpha \frac{U^2}{A^2} \tag{4.1}$$

The square of glottal area is an alternative indicator of airflow based on a model of laminar flow through a cylinder (Poiseuille flow) if the pressure drop across the glottis, viscosity (η) and glottal length (L) are constant:

$$U = \frac{\Delta P}{8\eta L / \pi A^2} \alpha \ \Delta P A^2 \tag{4.2}$$

The minimum of the first derivative of these two indicators of airflow with respect to time provides a comparative estimate of maximum flow declination rate. In order to obtain smooth derivatives, they are taken analytically from between third and sixth order polynomials that approximate the glottal area and glottal area squared curves with correlation coefficients greater than 0.99. Contact force between the vocal folds is calculated as the sum of point forces acting on medial nodes by the contact plane in the glottal midline. Mechanical stresses in the different vocal fold tissues are examined at the medial midmembranous region where vocal fold pathologies often manifest. Particular attention is paid to normal stress in the three coordinate directions and vertical shear stress on the plane parallel to the collision plane during collision since these have been identified as candidate stresses for vocal fold tissue damage (Chapter 3).

RESULTS

Model results show substantial variation with changes in SLP stiffness. Increases in SLP stiffness decrease the maximum glottal opening and the height of the mucosal wave at the onset of vocal fold closure (Figure 4.2). This decrease in glottal opening corresponds with decreased maximum airflow, an indicator of voice intensity, as estimated using the square of glottal area (Figure 4.3a) or glottal area (Figure 4.3b). Increases in SLP stiffness increase the maximum normalized flow declination rate, a voice quality parameter, as estimated by the first derivative of normalized glottal area squared or normalized glottal area (Figure 4.3c).

The finite element model also predicts the mechanical forces that load the vocal fold during closure and collision. Increases in SLP stiffness increase the maximum contact force between the vocal folds, as estimated using the sum of point contact forces between

the medial vocal fold surface and the contact plane. Increases in maximum contact force are paralleled by decreases in maximum volume as estimated by glottal area squared (Figure 4.4).

Alterations in SLP stiffness alter the nature and magnitude of mechanical stresses. Collision between the vocal folds is associated with compression in all three normal directions in the medial epithelial and SLP layers in the midmembrous region. The magnitudes of these compressive stresses are greater in the epithelium than the SLP and are proportional to SLP stiffness (Figure 4.5a). Collision between the vocal folds is associated with an increase in shear stress on the plane of collision in the vertical direction in the medial epithelium and SLP adjacent to the midmembrous region, the magnitude of which varies directly with SLP stiffness (Figure 4.6a). The maximum open position of the vocal fold is associated with high epithelial tension along the length of the vocal fold (σ_{yy}) in models with low SLP stiffness. The σ_{yy} stress in the medial SLP in the maximally open position of the vocal fold varies in the opposite manner (i.e. it increases as SLP stiffness increases) (Figure 4.7a). All stresses in the epithelium are related to strain by the same elastic constant in all models. Therefore epithelial stress trends indicate epithelial strain trends. Stresses in the SLP are related to strain by model specific elastic moduli. The magnitudes of all deformations examined in the midmembranous, medial SLP (normal compression during collision, shear deformation during collision, longitudinal tension prior to collision) decrease as SLP stiffness increases (Figures 4.5b, 4.6b, 4.7b).

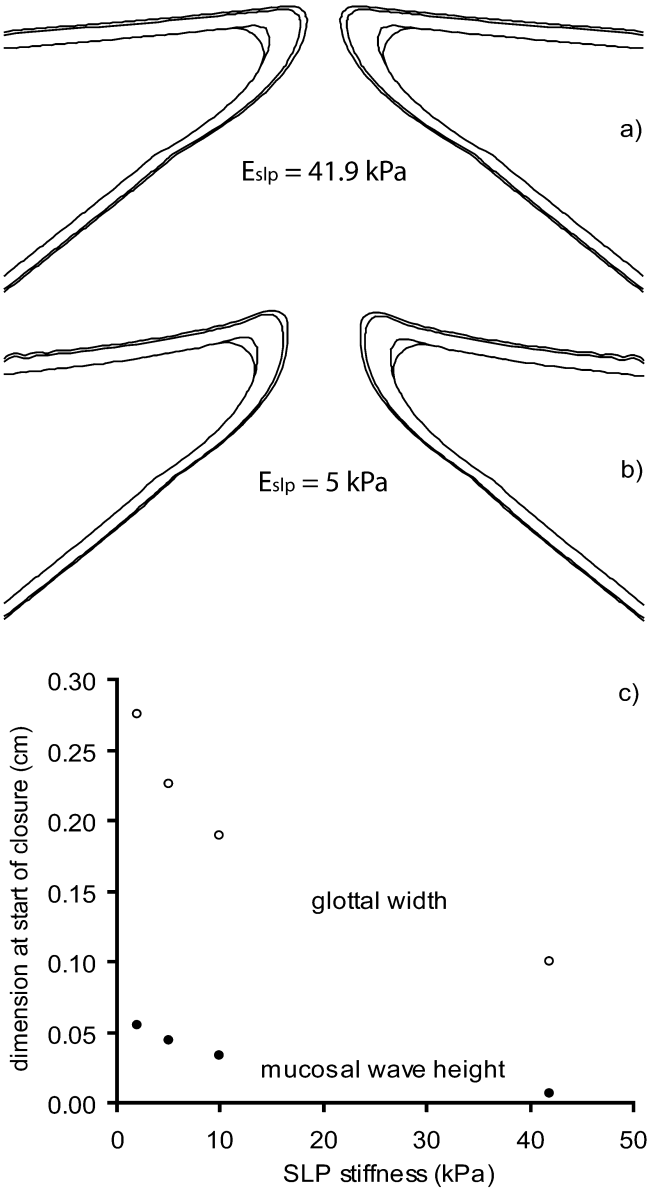

Figure 4.2: Effect of SLP stiffness on vocal fold deformation in the midmembrous region at the start of glottal closure as predicted by a layered finite element model
(a) SLP stiffness is equal to the epithelial stiffness. **(b)** SLP stiffness is approximately eight fold less than the epithelial stiffness. **(c)** Increasing SLP stiffness causes decreases in glottal width (i.e. the distance between the edges of the two vocal folds in the midmembranous region) and mucosal wave height (i.e the height of the upturned vocal fold edge). Each data point is from a model with a set SLP stiffness. The highest SLP stiffness is equal to the epithelial stiffness used in all models.

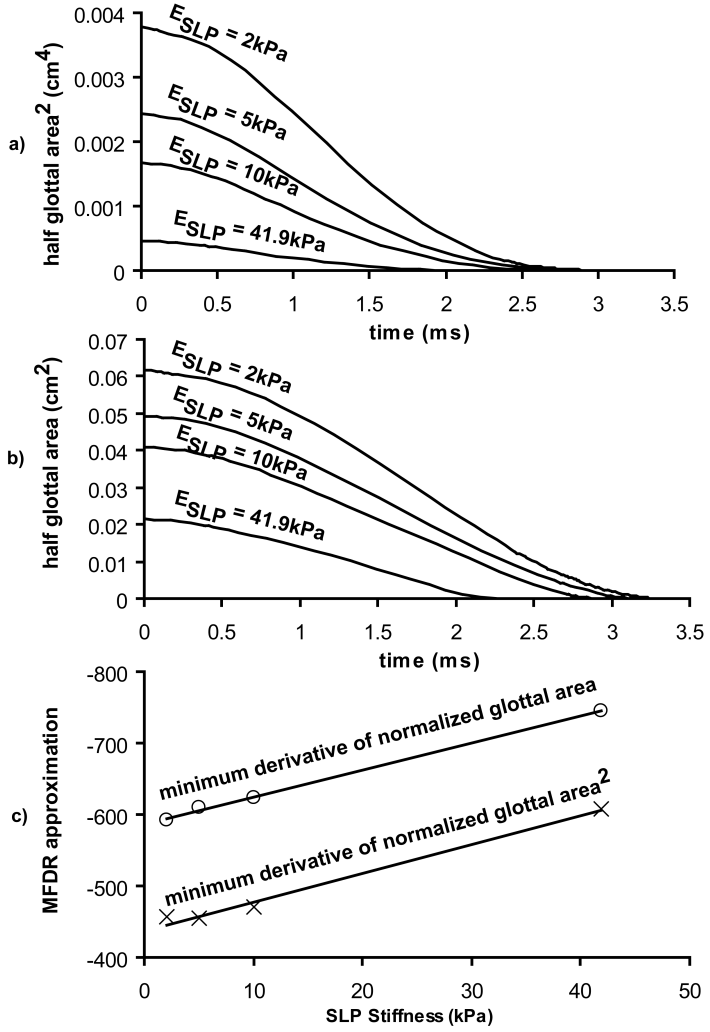

Figure 4.3: Effects of SLP stiffness on the falling portion of the aerodynamic waveform as estimated by glottal area squared and glottal area as predicted by a layered finite element model

(a) Increases in SLP stiffness cause a decrease in the amplitude of the glottal area squared waveform and by extension a decrease in voice intensity. Each curve illustrates the results for a single model. The discrete data curves are indistinguishable from sixth order polynomial fits of the data ($r^2 > 0.99$) **(b)** Increases in SLP stiffness cause a decrease in the amplitude of the glottal area waveform and by extension a decrease in voice intensity. Each curve illustrates the results for a single model. The discrete data curves are indistinguishable from third to fifth order polynomial fits of the data ($r^2 > 0.99$) **(c)** MFDR approximations based on the minimum derivatives of the polynomial fits of the data curves in (a) and (b).

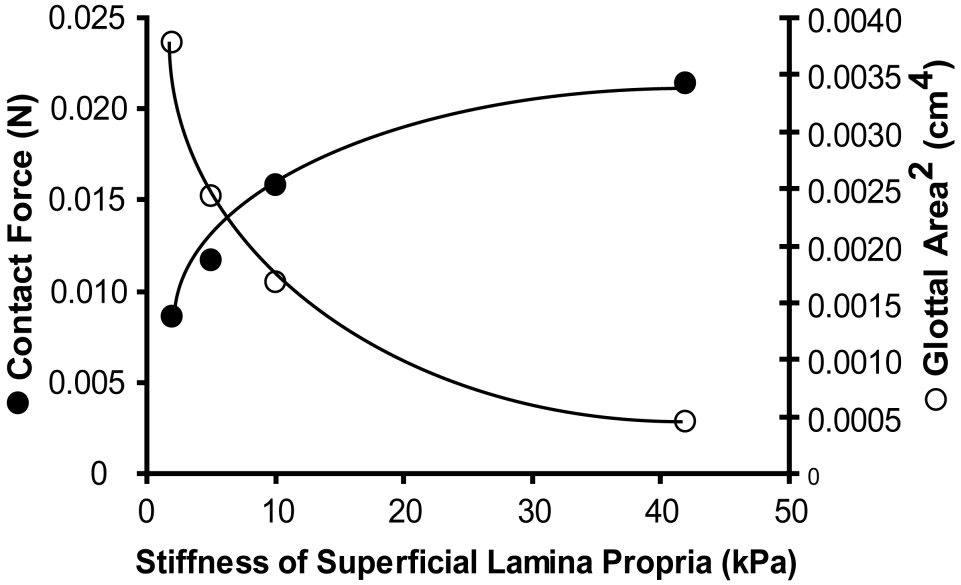

Figure 4.4: Effect of SLP stiffness on maximum contact force between the vocal folds and glottal area^2 as predicted by a layered finite element model
Increases in SLP stiffness are associated with an increase in the maximum contact force, a decrease in glottal area^2 and by extension a decrease in voice intensity.

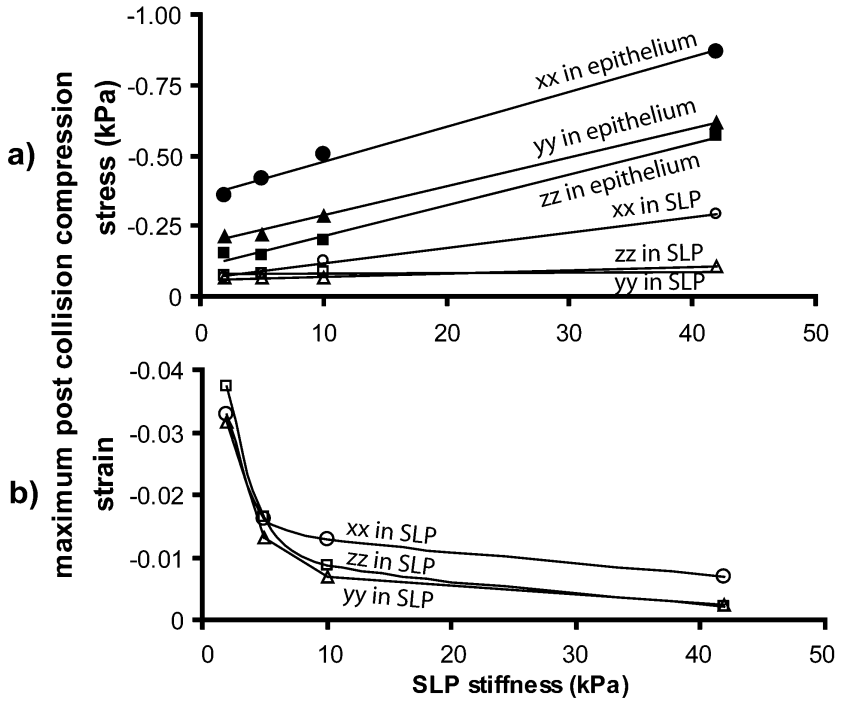

Figure 4.5: Effect of SLP stiffness on maximum normal compression in the midmembranous region during vocal fold collision as predicted by a layered finite element model

(a) Increases in SLP stiffness are associated with increases in normal compressive stress in all three coordinate directions in the epithelium and increases in normal compressive stress perpendicular to the plane of collision (*xx*) in the SLP. **(b)** Increases in SLP stiffness are associated with decreased normal compressive strains in the SLP. The epithelial strain trend is identical to the epithelial stress trend since the stiffness value was the same for all models.

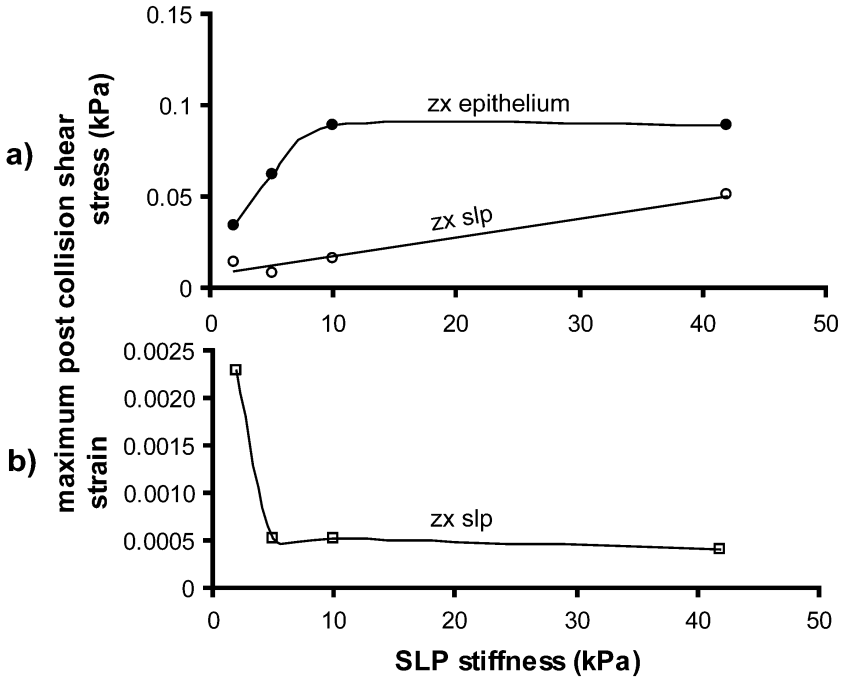

Figure 4.6: Effect of SLP stiffness on maximum vertical shear stress on the plane parallel with the plane of collision (*zx*) in the midmembranous region during vocal fold collision as predicted by a layered finite element model
(a) Increases in SLP stiffness are associated with increases in shear stress in the epithelium and the SLP. **(b)** Increases in SLP stiffness are associated with decreased shear strains in the SLP. The epithelial strain trend is identical to the epithelial stress trend since the stiffness value was the same for all models.

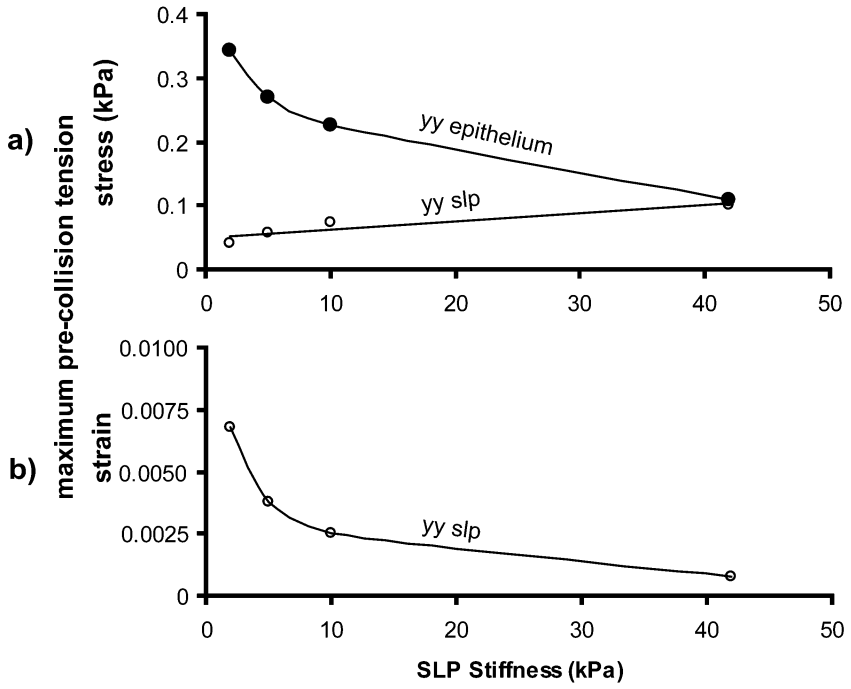

Figure 4.7: Effect of SLP stiffness on maximum longitudinal (*yy*) tension in the midmembranous region prior to vocal fold collision as predicted by a layered finite element model

(a) Increases in SLP stiffness are associated with decreased longitudinal stress in the epithelium and in increased longitudinal stress in the SLP. **(b)** Increases in SLP stiffness are associated with decreased longitudinal strains in the SLP. The epithelial strain trend is identical to the epithelial stress trend since the stiffness value was the same for all models.

DISCUSSION

The model predicts the behavior of four layers of tissue, each of which is defined using isotropic linear elastic material parameters, during vocal fold closure and collision. Model predictions agree with published experimental and theoretical data. Vibration amplitudes on the scale of millimeters for a subglottal pressure of 1 kPa (Figure 4.2c) are in accordance with those observed using high speed imaging of canine larynges (Berry et al., 2001a). Contact force magnitudes on the order of 10-20 mN for a subglottal pressure of 1 kPa (Figure 4.4) compare closely with experimental measurements of 12 mN (Jiang and Titze, 1994) and theoretical predictions of 10-16 mN (Chapter 2), both for a 1 kPa subglottal pressure. Predicted normal stresses during collision for a model with a stiff SLP are of the same pattern and order of magnitude but less than those predicted using a homogeneous finite element model (Chapter 2). This may reflect the use of layer distinct material properties in the current model. The predicted direct relationship between SLP stiffness and epithelial normal stress follows the prediction of a simple lumped mass model (Chapter 3).

Models of vocal fold tissue mechanics provide a means of interpreting indirect data that is obtained during clinical examination of vocal fold health, such as stroboscopic images and acoustic recordings. Model prediction of an inverse relationship between SLP stiffness and mucosal wave height (Figure 4.2c) supports a common interpretation of absent mucosal waves in stroboscopic images as SLP pathology, including regional stiffening caused by scar. Predictions of vocal fold margin deformation during closure and collision indicate that increases in SLP stiffness contribute to a decreased maximum glottal area squared (Figure 4.4a), an indicator of voice intensity, for a given subglottal

pressure, and suggest that increased vocal efficiency (the ratio between oral sound power and the product of subglottal pressure and flow) is an indicator of decreased SLP stiffness. This could be used in clinical assessment since noninvasive pressure sensors in the oral cavity can approximate both oral and subglottal pressures. Indirect assessment of SLP stiffness is useful since the SLP is a target for surgical manipulation (Zeitels et al., 2002). However, the current pool of data is insufficient since variables such as geometry that may contribute to the mucosal wave and vocal efficiency have not been explored. A complete exploration of the vocal fold tissue parameter space has the potential to create a library that connects clinical measurements with tissue properties in order to augment clinical diagnosis.

In addition to assisting with the interpretation of indirect clinical data, understanding the link between vocal fold tissue parameters and voice can guide surgical planning. Evaluation of glottal area dynamics using a model of vocal fold tissue mechanics predicts changes in voice intensity and maximum flow declination rate due to changes in SLP stiffness (Figure 4.4). These parameters could be used as inputs to a physiologically based speech synthesis program in order to predict voice waveforms specific to vocal fold tissue alterations. The combination of a detailed tissue model and voice synthesis would form a model capable of predicting surgical outcomes that could be used to test proposed manipulations. Quantification of the relationship between glottal closure dynamics and the falling arm of the aerodynamic waveform, for example using in vivo photoglottographic studies or by including aerodynamics in a theoretical model, is a necessary step towards achieving this goal. Optimizing the computation of the tissue

mechanics is also necessary so that the effect of multiple manipulations could be predicted in a reasonable time scale.

Relationships between SLP stiffness and mechanical stress indicate the role of SLP stiffness in determining tissue mechanical injury risk. Increases in compressive stress (Figure 4.5a) and vertical shear stress on the plane parallel to the plane of collision (Figure 4.6a) in the medial midmembranous epithelium during collision that are caused by SLP stiffness increases suggest that increasing SLP stiffness increases the risk of epithelial failure in compressive or shear modes. The former may result in changes in epithelial gene expression (Ressler et al., 2000) that lead to changes in protein synthesis and secretion in nearby fibroblasts (Swartz et al., 2001). The latter may manifest as basement membrane damage (Gray and Titze, 1988). Injury risk increases as a result of SLP stiffness increases are associated with decreases in voice intensity as indicated by maximum glottal area squared or glottal area (Figure 4.3). These contrast with stress associated risk increases due to increases in subglottal pressure (Chapter 3), which are associated with increases in voice intensity. Thus voice intensity alone does not indicate injury risk. However, injury risk as a result of SLP stiffness increases are associated with increases in collision force between the vocal folds (Figure 4.4), as are those due to increases in subglottal pressure. This supports the use of interfold collision forces to assess injury risk.

Low SLP stiffness results in a pre-collision tensile stress in the epithelium (Figure 4.7a) that has not been observed in models that combine the epithelium and SLP into a single layer. This tensile stress occurs along the medial edge of the vocal fold when it is in the fully open position, much like tension in a vibrating string, and acts to separate adjacent

epithelial cells and impair wound healing (Waters et al., 2001). If the SLP is the same stiffness as the epithelium it provides support for the deformation by effectively increasing the cross sectional area of the vibrating string and therefore minimizes this tensile stress. Thus, increased SLP stiffness decreases injury risk due to epithelial tension.

Increases in SLP stiffness cause increases in post collision stresses in the SLP to a lesser degree than in the epithelium (Figures 4.5a, 4.6a). However, lower stress magnitudes in the SLP than the epithelium do not translate into lower injury risks since the two tissues are distinct and likely respond to stress differently. Therefore increases in SLP stiffness are associated with an increased risk of compressive and shear failure in the SLP due to stress. As in the case of the epithelium these stress increases are accompanied by increases in collision force. Another possible indicator for injury risk is strain. Increases in SLP stiffness are associated with decreases in compressive and shear mechanical strain in midmembranous SLP, and therefore decreased risk of injury due to strain induced failure, a trend that is opposite to the stress trend. Which of stress or strain is most concerning is not clear. If the damage is physical failure of proteins then stress in the SLP proteins that support forces is likely the most important quantity. If the damage is functional then strain of the fibroblasts and other cellular components that deform with the matrix but likely support little force is the most important quantity. Clever experiments involving synthesized SLP are necessary to determine the relevant modes of failure.

A finite element of vocal fold tissue model predicts that superficial lamina propria stiffness plays a role in determining voice output, its own injury risk and the injury risk of

adjacent tissues. In the design and selection of SLP implant materials consideration needs to be given to minimizing SLP strain and epithelial longitudinal tension by increasing SLP stiffness and minimizing collision induced epithelial and SLP compressive and shear stresses and maximizing vocal efficiency by decreasing SLP stiffness. Other considerations that have not been addressed here include the viscous SLP properties (Chan and Titze, 1999b) that contribute to phonation threshold pressure (Titze et al., 1995), regional variations in SLP stiffness and SLP geometry. Precise recommendations will require detailed characterization of the nonlinearity of SLP material properties at voicing frequency and identification of relevant modes of tissue injury.

CHAPTER 5: MEASUREMENTS OF VOCAL FOLD COLLISION FORCES DURING PHONATION[1]

INTRODUCTION

Collisions between the vocal folds during phonation have implications for vocal fold injury and voice quality. In the former instance, the application of high forces to the medial surfaces of the vocal folds may cause tissue injury that manifests as organic pathologies (Gunter, 2003a;Titze, 1994). In the latter instance glottal closure is the tissue correlate of maximum airflow declination rate, which relates to voice quality perceptions (Holmberg et al., 1988). Experimental measurements of the forces transmitted between human vocal folds during phonation have the potential to improve our understanding of vocal fold collision mechanics.

In vivo measurements of intra vocal fold collision forces during human phonation are challenging to make. Placing a sensor between the vocal folds in vivo can be achieved by topically anesthetizing the subject's pharynx and larynx, mounting the sensor on a

[1] This chapter will be submitted as Gunter, H.E., Howe, R.D., Kobler, J., Zeitels, S.M., Hillman, R.E. (2003) "Measurements of vocal fold collision forces during phonation: Methods and preliminary data" to the Journal of Speech, Language and Hearing Research

curved canulla and visualizing placement between the vocal folds using transoral endoscopic images (Hess et al., 1998;Yamana and Kitajima, 2000). These studies report membranous vocal fold collision pressures between 1 and 4 kPa and examine the effects of qualitative changes in register, pitch and intensity. However, they also report that the presence of a sensor between the vocal folds tends to disrupt in vivo phonation, thereby eliminating the parameter that is being measured. It is likely that even when phonation is maintained that the deformation of the tissue around the sensor introduces measurement artifacts. A similar artifact concern applies to in vitro measurements in whole canine larynges using sensors between 0.4 mm and 1.8 mm thick with 2 mm diameters (Berry et al., 2001b;Jiang et al., 2001a). The hemilarynx preparation used by Jiang and Titze (1994) addresses this concern. In this preparation a single vocal fold vibrates against an instrumented plexiglass surface. The active sensor surface is flush with the medial surface of the plexiglass and therefore the collision plane remains flat. Hemilarynx phonation is a reasonable approximation of that seen in whole larynges (Jiang and Titze, 1993). However, impact force data collected from excised canine larynges are not necessarily equivalent to human impact force magnitudes due to differences in anatomy, physiology and tissue viability.

We report a novel method for obtaining measurements of in vivo vocal fold collision forces during human phonation. This method uses subjects with hemilarynx-like anatomy (i.e. one rigid, medialized vocal fold). A custom designed low profile force sensor covers the surface of the rigid fold. This reduces measurement artifacts by maintaining flat collision plane topography. The quantitative force measurements characterize the in vivo mechanical environment of human vocal fold tissue, provide data

with which to validate models of vocal fold mechanics and have implications for investigating mechanical injury of vocal fold tissue.

METHODS

Collision force sensor design, construction and characterization

We designed a force sensor consisting of a transducing element, analog electronics, and mechanical components for transoral endolaryngeal placement (Figure 5.1). The transducing element is a 0.29 mm thick flat rectangle with dimensions of approximately 10 mm by 15 mm (Figure 5.2). The active part of the transducer is composed of two stacked pieces of 28 μm thick metalized piezo-electric PVDF film (Measurement Specialties Inc.; Fairfield, NJ), with leads attached to the outsides of the stack and between the two pieces of film. In response to force across the stack, the piezo-electric film deforms and generates an electric charge difference across the film that is amplified by subsequent electronics. Kapton polyimide film with pressure sensitive silicone adhesive (Kapton Tape Inc.; Torrence, CA), applied to both sides of the piezo-electric film stack, provides electrical insulation and protection from the in vivo saline environment. An outer coating of FDA approved silicone elastomer (MED10-6605, Nusil Technology, Carpinteria, CA), applied by dipping, provides additional insulation.

The charge difference across the stack of piezo-electric film is converted to a voltage signal using simple analog electronics (Figure 5.3a). The three leads connected to the piezo-electric film stack are connected to insulated and shielded twisted three conductor cable that is 2 mm in diameter (CW 2516 Rev 1, Cooner Wire; Chatsworth, CA). The signals from the outside of the stacks are tied to ground, and the signal from the middle of the stack is fed through a charge amplifier, a high pass filter with a 30 Hz corner

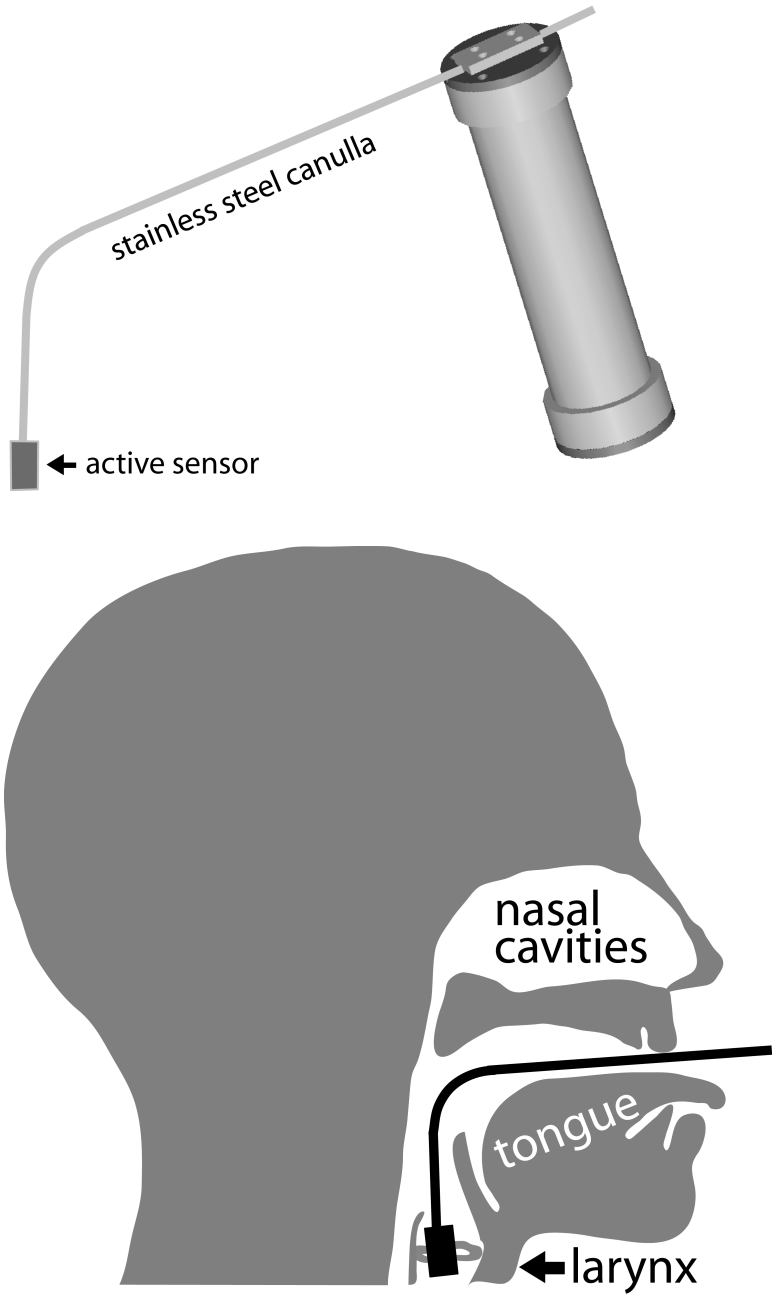

Figure 5.1: Mechanical housing of sensor for measuring in vivo vocal fold collision forces and placement of the sensor between the vocal folds
Top panel illustrates the construction of the sensor housing. The stainless steel canulla is rigid and carries the leads from the active sensor to the analog electronics, which are housed in the sensor handle. The examiner uses the handle to guide the active sensor through the mouth and pharynx to achieve endolarygeal placement as shown in the lower panel.

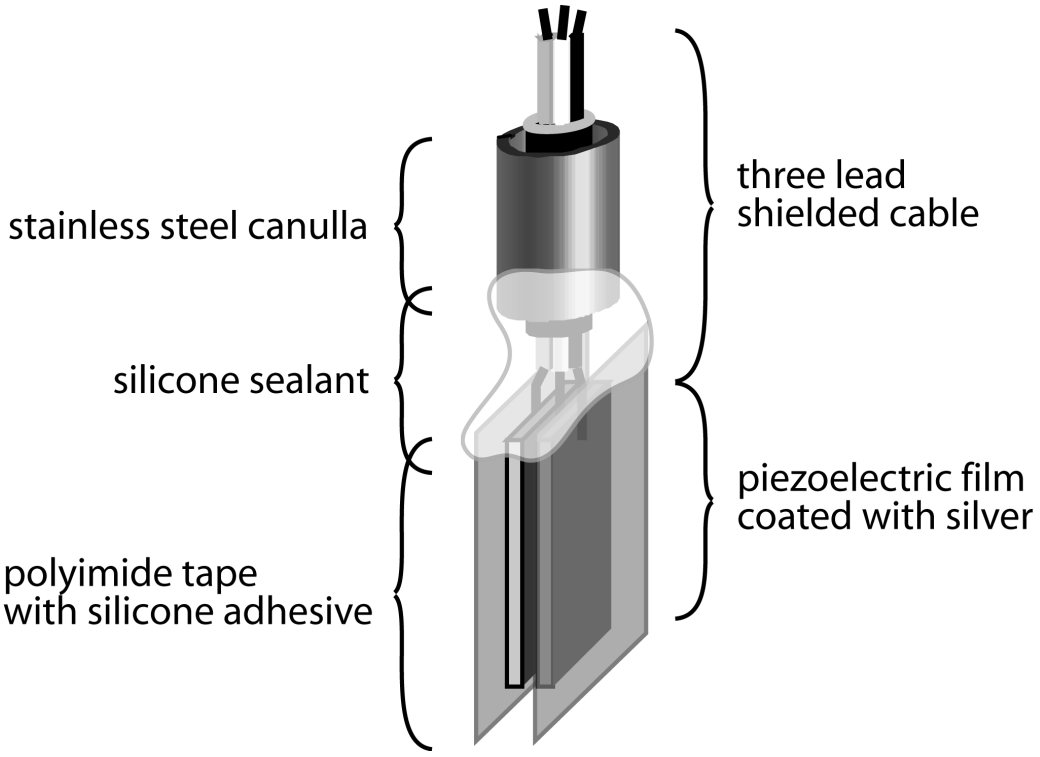

Figure 5.2: Construction of the active area of a low profile force sensor for measuring vocal fold collision forces in vivo
Piezoelectric film generates a charge difference between its silver coated faces in response to applied force. Film pieces are oriented with opposite polarities and the outer surfaces are connected to ground in order to minimize noise. The cable carries this signal away from the active sensor. Polyimide tape protects the piezoelectric film from a saline environment. Silicone sealant provides strain relief. Stainless steel canulla provides rigid support for the cable and sensor.

frequency and two inverting amplifiers with adjustable gain, before being carried in shielded twisted pair cable to the data acquisition system. Two 10.5 V alkaline batteries (Duracell PC 177A; The Gillette Company; Alpharetta, GA) power the circuits. The shield of the transducer cable is continuous with a shield that surrounds the electronic circuitry and the output cable shield. The voltage output of the sensor is proportional to the force applied across the sensor and is noise limited to 20 mV (2.5 mN). Rapidly lifting a known mass off the surface of the sensor results in a transient voltage response. Linear regression of the amplitude of these voltage responses as a function of the magnitudes of the step decreases in force that caused them generates linear calibration curves with calibration constants of approximately 7.9 mV/mN (Figure 5.3b). A high pass filter before the final amplifying stage of the circuit has a corner frequency of 30Hz and limits the response of the system to frequencies below this cutoff (Figure 5.3a). Theoretically there is no upper bound on the frequency response. Flat response of the electronics has been verified up to 25kHz. The sensor is also sensitive to bending and changes in temperature. The former is minimized by the rigidity provided by the polyimide insulation. The latter is significant for the initial 200ms of voicing, during which time the sensor equilibrates with the temperature of the warmer, exhaled air stream (Figure 5.4).

The mechanical components of the sensor provide structural support and facilitate endolaryngeal placement (Figure 5.1). The cable leading from the transducer to the electronic circuits is carried in a curved 12 gauge stainless steel canulla that is long enough to introduce the transducer transorally into the endolarynx. The transducer is bonded to the distal end of the canulla with silicone adhesive to provide additional

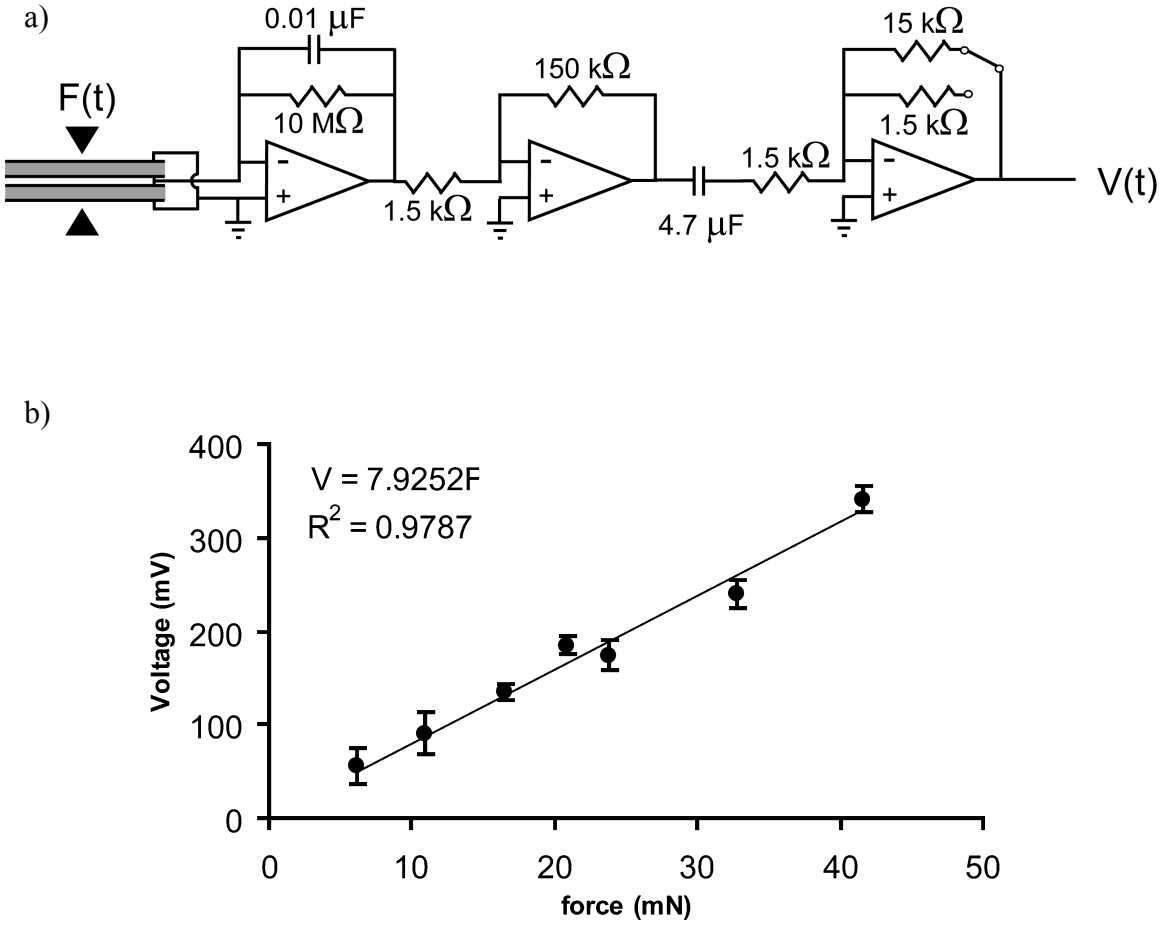

Figure 5.3: Analog processing of signal from pressure sensitive piezoelectric film to produce voltage output that is proportional to force input
(a) Analog circuitry that converts the charge difference across the piezoelectric field in response to applied force to a time varying voltage consists (from left to right) of a charge amplifier, a noninverting amplifier with set gain, a high pass filter and a noninverting amplifier with adjustable gain. **(b)** Sample calibration curve for amplitude of sensor response to step decreases in force. Each data point is the mean for at least 5 measurements. Error bars are standard deviation. Linear regression parameters are shown in the upper left corner.

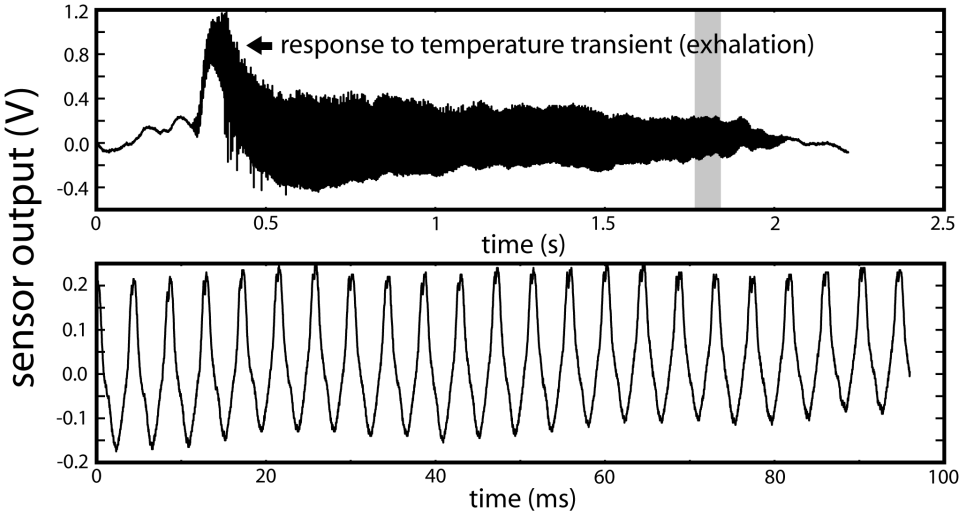

Figure 5.4: Voltage output of a low profile force sensor placed between human vocal folds during production voice
Top panel illustrates sensor output during 2 seconds of phonation at approximately 233 Hz. The low frequency transient is due to the temperature increase caused by exhaled air. The high frequency component is at the same frequency as voice production. The lower figure shows the high frequency vibrations from the shaded region of the top panel. Note that compressive forces (i.e. collision) generate negative voltage from the sensor.

insulation and strain relief. The proximal end of the canulla is attached to one end of an aluminum cylinder. This cylinder serves as a handle for manipulating the sensor and as housing for the electronic circuits. Two switches on the bottom of the handle control power to the circuits and gain of the second amplifying stage.

Experimental setup

During experiments to measure vocal fold collision forces, endoscopic and acoustic data were collected in addition to the intraglottal force data. Videolaryngoscopic images were obtained using a rigid transoral endoscope (Rhino-Laryngeal Stroboscope model 1900; Kay Elemetrics; Lincoln Park, NJ) and a system that includes halogen (constant) and xenon (strobe) light sources, a CCD camera with endoscope coupler, and a super VHS tape deck. These images were used during the experiment to monitor sensor placement and voice quality. Acoustic data was collected using a microphone (ECM50PSW, Sony) placed approximately 30 cm from the subject's mouth. Microphone output was calibrated using a sound pressure level meter for three different sound intensities produced using a 150 Hz buzzer. A calibration equation for each subject was obtained by performing linear regression on the voltage-SPL data points. Electroglottographic (EGG) waveforms were collected for an initial subject's recordings in order to assess the timing of the force waveform, but this practice was not continued due to concerns regarding interference between the EGG system and the force sensor.

Force data was collected using the force sensor described above when it was positioned between each subject's vocal folds. Calibration data were collected either prior to or following data collection from each subject. Calibration coefficients valid for a single experiment were obtained as described in the previous section. These coefficients varied

by up to 10 % between experiments. Audio and force sensor data were digitized at 50kHz using a 12 bit analog to digital converter (Digidata 1200A, Axon instruments, Union City, CA).

Experimental protocol

The experimental protocol, including use of the collision force sensor, was approved by the Massachusetts Eye and Ear Infirmary Human Subjects Committee (Protocol number 01-09-050), and by the Harvard University Committee on the Use of Human Subjects in Research. Prior to data collection, each subject read and signed an approved consent form that described the nature of the project, the measures to be made, and the potential risks and benefits of their participation. Subjects were instructed not to eat or drink for at least 1 hour following their participation in the study.

Three males and one female who had undergone laryngeal reconstruction surgery subsequent to surgical excision of laryngeal cancer participated in the study. These subjects produce voice using one vibrating and nonvibrating, reconstructed vocal fold. They were selected based on good conversational voice quality, minimal vibration of the reconstructed fold during phonation and minimal constriction of the supraglottal structures. One male subject with normal laryngeal anatomy was also a study participant.

Topical anesthesia minimized subject discomfort. The pharynx was sprayed with 14% benzocaine prior to endoscope insertion. 4% lidocaine (xylocaine) was swabbed and dripped on the endo-larynx walls under endoscopic guidance until there was no response to instrument palpation of the vocal fold surface. Evidence that anesthesia was

insufficient or wearing off, for example gagging, was grounds for terminating data collection.

Following anesthesia, data collection was initiated. Subjects held their tongues with a piece of gauze to maximize laryngeal access. The examiner inserted a camera-coupled rigid laryngoscope transorally to visualize the larynx. Using the endoscopic images on the video monitor for guidance, the examiner inserted the collision force transducer between the vocal folds such that it rested against one vocal fold. Throughout the experiment sensor placement was refined based on auditory perception of voice quality, and phonation quality as visualized with stroboscopy.

The subjects phonated in response to instructions from the examiner while the force sensor was in place. The phonation tokens requested of the subject include pitch/volume pairs (normal/normal, high/normal, low/normal, normal/high, normal/low), pitch glides at constant volume and volume glides at constant pitch. In all cases tokens were repeated until good voice quality, as judged by the experimental team, was achieved. Following each 1-2 minute segment of data recording all instrumentation was removed and the subject was given a chance to rest. Collection of data was terminated when the subject was no longer able to tolerate sensor and scope placement due to anesthesia wearing off or when sufficient data was collected.

Data processing and analysis

A primary goal was to restrict analysis to data segments with both good quality voice and good sensor placement. Two members of the experimental team rated the quality of each phonation segment as poor, acceptable or good during review of the video and audio

experimental recordings while blinded to the sensor and audio waveforms. Thus, voice quality judgments were based on a combined assessment of both audio and stroboscopy recordings. Judgments of sensor placement accuracy were also based on stroboscopic images.

For recorded samples judged to have good voice quality and good sensor placement the data waveforms were examined and a consistent segment with at least 5 consecutive cycles of vibration was selected. A script executed in Matlab was used to estimate frequency, audio amplitude and force amplitude from these segments. Frequency estimation was based on a fourier transform of the audio signal. Audio and force amplitudes were based on averaging the peak and valley magnitudes for all cycles in the segment. Audio and force amplitudes in volts were converted to dB and mN respectively by applying the appropriate derived calibration factors. In order to do this it was assumed that the lowest force was equal to 0 N, which is consistent with experimental measurements of impact force using in vitro canine hemilarynges.

RESULTS

Data collection was attempted from four subjects (3 males and 1 female) who had undergone vocal fold reconstruction surgery and one male subject with no history of laryngeal pathology or surgery. The sole female subject was unable to tolerate passage of the sensor through her pharynx. In the three male subjects who had undergone laryngeal surgeries, the examiner was able to consistently place the sensor in the glottis and rest it against the immobile fold, such that the sensor covered 50-75% of the membranous vocal fold (i.e. anterior to the vocal process), while the subject produced voice (Figure 5.5). In one male subject who had undergone laryngeal reconstruction surgery supraglottal

constriction impaired visualization of his vocal folds such that voice quality and sensor placement could not be reliably evaluated. The examiner was able to successfully place the sensor between the vocal folds of the male subject with no history of laryngeal surgery. For the normal subject, two strategies resulted in good quality phonation. One involved stabilizing the sensor in the center of the glottis by placing the posterior half between the adducted arytenoid cartilages. The other involved halting the vibration of one of the vocal folds by applying lateral force to it using the sensor.

Data was collected in approximately 100-second intervals between which the sensor and laryngoscope were removed from the subject's larynx and pharynx. This limit was determined by mucous collection, fogging of scope and subject tolerance. Each of the male subjects participated in 3 or 4 intervals of data collection. Sensor placement and voice quality were good during voice segments that were produced in response to relative instructions (i.e. lower pitch, louder volume etc.) and crescendo requests (i.e. same pitch, increasing volume). Sensor placement during glides (i.e. changing pitch) was poor due to difficulties adjusting the sensor to account for vertical movement of the larynx. A sample segment of the variety selected for analysis with a frequency of 137 Hz is shown in Figure 5.6. EGG data was initially collected simultaneously to help guide the interpretation of the force sensor waveform but was not collected for all subsequent participants.

In the normal subject one voice segment was identified with good sensor placement and good voice quality. In this segment the collision force amplitude was 95 mN. Other segments with good voice quality were judged unsuitable for analysis due to the interarytenoid location of part of the sensor.

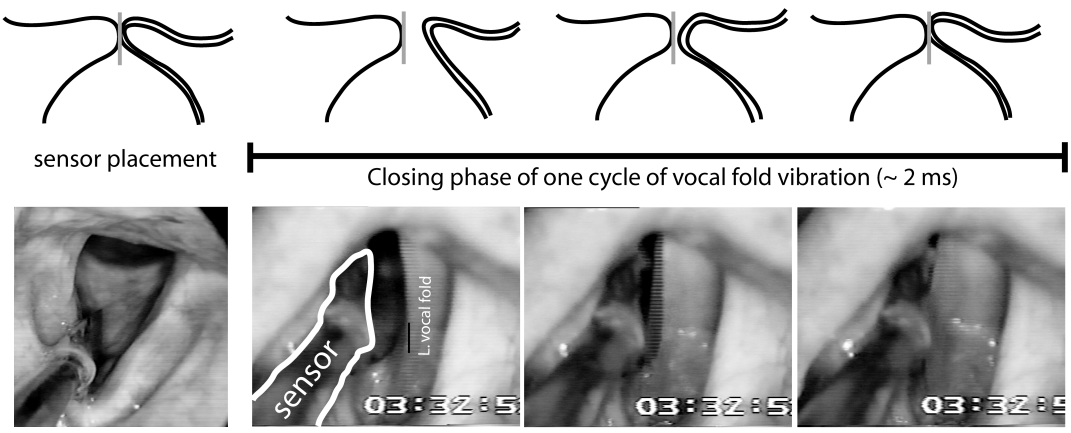

Figure 5.5: Production of voice by a subject while a low profile sensor is rested against his one rigid fold
The rigid fold is on the left hand side of the images. The black line drawings illustrate coronal sections through the midmembranous vocal folds. The vertical gray lines illustrate sensor placement. The laryngeal images were obtained using transoral endoscopy with stroboscopy.

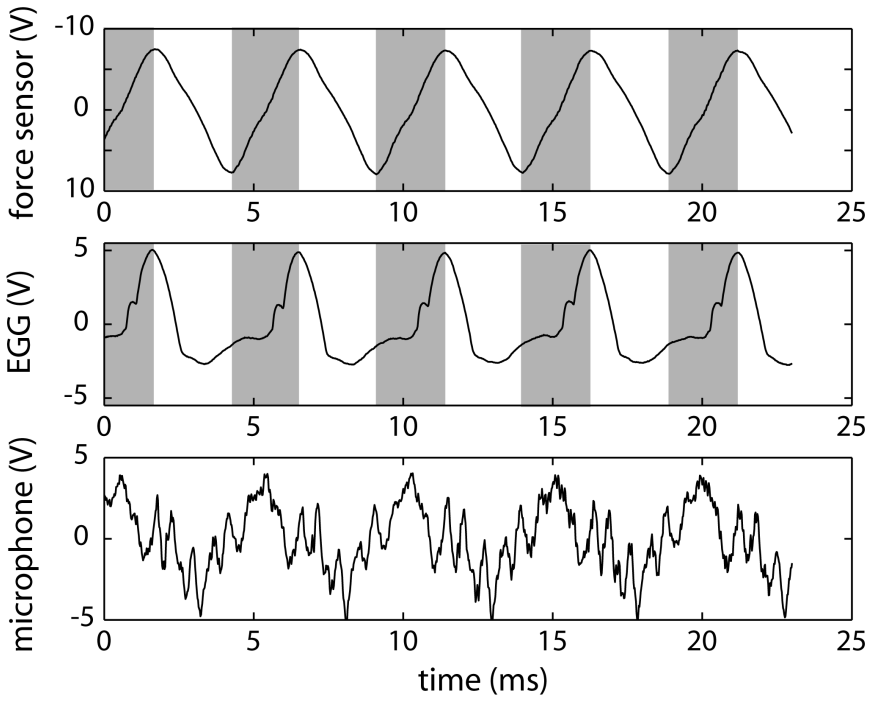

Figure 5.6: Segment of simultaneously acquired intraglottal force, EGG and audio data during voice production.
The gray bars indicate the rising arm of the force waveform, which indicates compression.

In the two male subjects who had undergone reconstruction surgery and for whom good visualization was possible 16 segments with good voice quality and good sensor placement with collision force amplitudes ranging from 5 to 42 mN were collected from subject one, and 21 segments with good voice quality and good sensor placement with collision force amplitudes ranging from 13 to 210 mN were collected from subject two (Figure 5.7). Planar regression analyses generate coefficients for force as a function of intensity and frequency (equation 5.1). The intensity coefficient (C_{PI}) is at least 10 fold greater than the frequency coefficient (C_{PF}) for both subjects (Tables 5.1 and 5.2)

$$Force = C_{pI} Intensity + C_{pf} Frequency + C_p \tag{5.1}$$

Linear regression analyses generate coefficients for collision force as a function of either intensity or frequency (equations 5.2, 5.3). The intensity coefficient (C_{LI}) is similar to that obtained in the planar regression analysis for each subject. Force correlates better with intensity than frequency (Tables 5.1, 5.2).

$$Force = C_{LI} Intensity + C_L \tag{5.2}$$

$$Force = C_{Lf} Frequency + C_p \tag{5.3}$$

Table 5.1: Regression analysis of vocal fold collision force as a function of voice frequency and voice intensity (subject 1)

Regression type	Intensity Coefficient	Frequency Coefficient	Correlation (R^2)
Planar	1.4 mN/dB	0.1 mN/ Hz	
Linear (Intensity)	1.4 mN/dB	-	0.69
Linear (Frequency)	-	-5×10^{-5} mN/Hz	0.03

Table 5.2: Regression analysis of vocal fold collision force as a function of voice frequency and voice intensity (subject 2)

Regression type	Intensity Coefficient	Frequency Coefficient	Correlation (R^2)
Planar	9.3 mN/dB	0.1 mN/Hz	
Linear (Intensity)	9.4 mN/dB	-	0.48
Linear (Frequency)	-	0.3 mN/Hz	0.04

DISCUSSION

This novel method of measuring human vocal fold collision forces in vivo minimizes the interference of sensor placement with voice. In vivo measurements of collision forces in three subjects are an improvement over previous in vivo measurements due to more consistent voice quality and reduction in artifacts due to vocal fold deformation around the sensor.

Glottal air pressure forces may confound the collision force measurements since air pressures in the glottis have the same order of magnitude as the collision forces and the sensor output reflects integrated force over the sensor surface. These forces can be distinguished by their phase, which can be identified via reference to the EGG signal (Figure 5.6). Air pressure is at a minimum at full glottal opening, and reaches a maximum following full closure (Alipour et al., 2001). Collision force is at a minimum at full opening and reaches a maximum at full closure, such that its peak leads the air pressure peak (Jiang and Titze, 1994). EGG signals are also at a minimum at full opening and reach a maximum at full closure. Therefore comparisons between the phases of the EGG and sensor peaks provide an indication of whether the force peaks measured are due to air pressures (sensor peak lags EGG peak) or collision forces (sensor peak matches EGG peak). The in-phase nature of the EGG and sensor peaks supports the hypothesis that the peak of the force sensor waveform represents the collision force peak

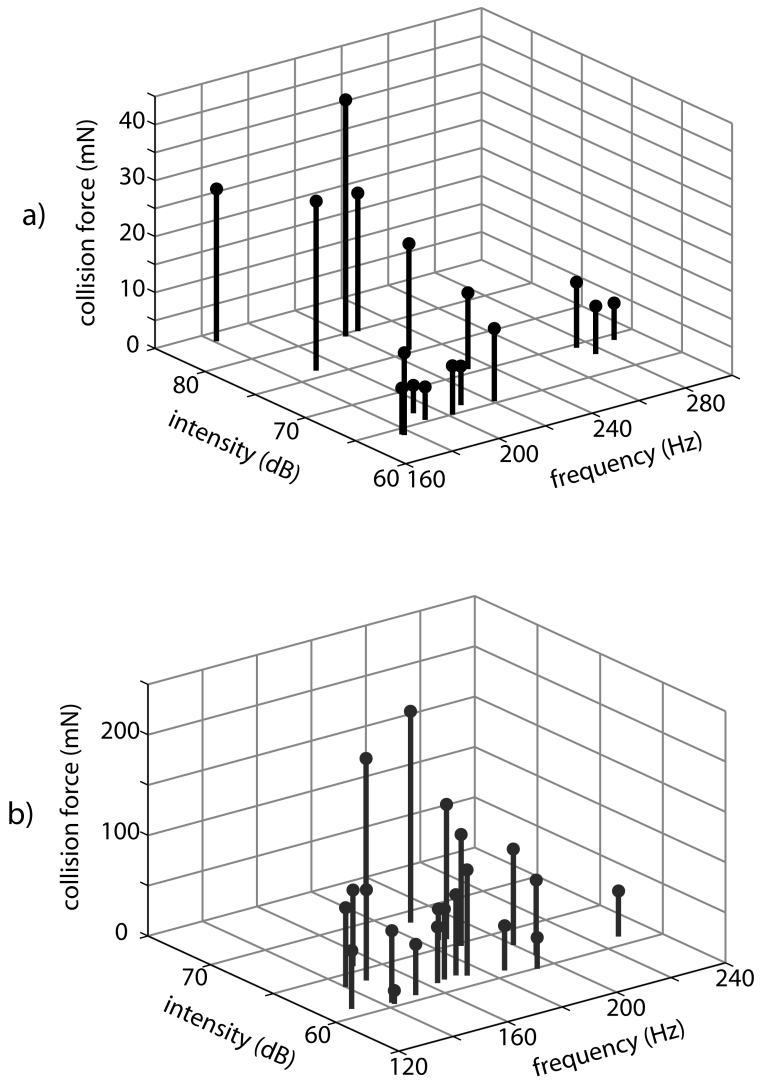

Figure 5.7: Scatter plots of vocal fold collision force, voice intensity and voice frequency data points measured in two male subjects
(a) Subject 1 **(b)** Subject 2

rather than an air pressure peak (Figure 5.6). This conclusion rests upon an assumption that the EGG and intraglottal force waveforms are synchronized, which is likely but unconfirmed. High-speed laryngoscopy could provide a reference against which to evaluate time delays between the EGG and force signals in order to confirm this assumption. The collision force peak may include a contribution from air pressure acting on the portion of the sensor that is not in contact with the vocal folds. It is likely that previously published measurements of vocal fold collision forces also include air pressure contributions due to use of sensors that extend beyond the collision area. Simultaneous subglottal pressure measurements would assist in the evaluation of the magnitude of air pressure contributions to the intraglottal force signal.

Theoretical studies also guide interpretation of the force sensor waveform since they distinguish contributions of collision force and air pressure to the intraglottal force waveform in their predictions. Three dimensional finite element models predict a period of noncollision during the initial moments of the closing phase followed by an increase in collision force that begins when the anterior and posterior aspects of the vocal folds come into contact, between 0.5 ms and 0.75 ms prior to complete closure (for a 127Hz vibration) (Chapter 2). Thus, these models predict a collision force rise time occupying approximately 10% of the vibration cycle. These theoretical results include all forces between the midmembranous folds. Since the sensor does not record forces at the extreme anterior and posterior aspects of the membranous folds, the time prior to the peak in the intraglottal waveform that is due to collision force is less than that predicted theoretically. A combination of elastic recoil (i.e. bouncing) of the tissue and forced separation by air pressure causes the collision force to decrease after full closure occurs.

In the experimental measurements, the force rise time occupies almost 50% of the vibration cycle (Figure 5.6). Comparison with theoretical results suggests that the nonzero intraglottal forces during the initial stages of the rising force waveform are due to air pressure forces, while those during the latter stage of closure are due to collision forces. Intraglottal force measurements at higher spatial resolution or simultaneous subglottal pressure measurements would guide further interpretation of the force sensor waveform. Visual data such as high speed laryngoscopy or kymography would assist in the alignment of force data with vocal fold movement.

The collision forces measured in both male subjects who had undergone laryngeal reconstruction surgery, and for whom visualization was good, span those obtained using a smaller sensor in a canine hemilarynx model (Jiang and Titze, 1994). These comparisons are valid despite the difference in sensor size since collision force between the vocal folds is concentrated in the midmembranous region, which is within the active area of both sensors (Jiang and Titze, 1994). The 5 fold difference between the maximum collision forces of each subject is consistent with the spread between different canine hemilarynges. The 10 fold differences between minimum and maximum collision forces in a single subject are consistent with changes achieved through manipulations of vocal fold length, adduction and subglottal pressure in the canine hemilarynx model. The collision forces measured at low intensities in these in vivo experiments are of the same order of magnitude of those obtained in other in vivo human experiments, for which there are doubts regarding measurement artifacts due to tissue deformation around thicker sensors and in which difficulties were encountered maintaining good voice quality (Verdolini and Hess, 1999). The collision force measurement obtained in the subject

with no history of laryngeal pathology is of the same order of magnitude as those obtained in the subjects who had undergone laryngeal reconstruction. This validates the use of the subjects with unique anatomy in whom measurements were technically easier to make as well as the use of the in vitro canine hemilarynx preparation, in which many more independent variables can be manipulated and controlled.

Acoustic intensity is a better predictor of collision force than frequency (Figure 5.7, Tables 5.1 and 5.2). Theoretical models demonstrate that collision force predicts certain compressive and shear mechanical stresses in the tissue that may disrupt tissue and manifest as pathology (Chapter 2). Therefore, the increase of force measurements with intensity suggests that mechanical stresses also increase leading to an increased risk of vocal fold injury. This complements theoretical evidence that demonstrates a dependence of mechanical stress magnitudes on subglottal pressure, which contributes to increasing intensity (Chapter 3) in explaining associations between vocal fold pathologies and loud voicing (Buckmire and Rosen, 2001).

The lack of trend between voice frequency and collision force may reflect complex strategies that are used to manipulate frequency rather than a lack of dependence of collision force on vocal fold length and stiffness. Theoretical results also fail to identify a direct relationship between pitch and mechanical stress and provide insight by demonstrating that the mechanical stresses that result from generation of a pitch depend on the muscle activation patterns used (Chapter 3). Lack of data on muscle activation patterns in our subjects prevents comparison with these predictions. The current analysis is restricted to correlations between dependent variables, since the true independent determinants of voice frequency, intensity and vocal fold collision force, such as

subglottal pressure, anatomy and muscle activities were not measured. More complex experiments involving tracheal puncture subglottal pressure measurements, three dimensional anatomical images, and EMG measurements of muscle activity, while experimentally challenging, have the potential to provide such data and improve our understanding of the determinants of collision force and by extension mechanical stress levels and injury risk. Such data would evaluate whether the 5 fold difference in the maximum collision forces between the two subjects reflects differences in vocal fold anatomy or voice technique, illuminate the intraindividual determinants of vocal fold collision forces and by extension injury risk and have implications for voice pathology prevention.

The method used to obtain estimates of vocal fold collision forces serves as a paradigm for characterizing the intraglottal mechanical environment since the low profile sensor is able to collect data during periods of normal phonation. We are not aware of published results using another method that has achieved good voice quality while taking intraglottal measurements in vivo. Enhanced sensors will expand the range of data that can be collected. One possibility is to decrease the active area of the current sensor without decreasing the size of the sensor in order to make point force measurements. This would provide a point estimate of collision force while maintaining the ease of placement of the current sensor and minimizing measurement artifacts due to vocal fold deformation around a smaller sensor. Other possibilities include an array of sensors in a plane such as those developed by Pawluk et al. (1998) that could measure spatial variations in contact force and estimate contact area.

The method used in this study was most successful in subjects with one rigid, medialized vocal fold that acted as a support for the sensor. Interarytenoid placement of the posterior end of the sensor offers an alternative method of stabilization in the subject with two vibrating vocal folds. However, measurements obtained using this method with the current sensor were difficult to interpret due to lack of understanding of the nature of interarytenoid forces during voice production and therefore inability to subtract them from the force sensor waveform in order to isolate the vocal fold collision force waveform. The addition of an inactive posterior extension to the sensor would provide an inactive mechanical structure that could be used for stabilization without contributing to the force sensor signal. This would facilitate making intraglottal measurements during phonation in normal subjects.

CHAPTER 6: CONTRIBUTIONS AND PROPOSED WORK

This thesis presents studies regarding the biomechanics of vocal fold tissue during voice production and provides insights into the role of solid mechanics in voice production and voice pathology development. Both the methods developed and the results presented in this thesis represent novel contributions to the fields of biomechanics and voice science. The results provide answers to some of the original research questions, and also provoke new queries.

METHOD FOR THEORETICAL STUDY OF VOCAL FOLD COLLISION

Theoretical models of vocal fold tissue mechanics are useful for exploring the interactions between many variables in voice production. However, maximization of geometric, material and aerodynamic detail is prohibitively computationally intensive. A new approach to theoretical models of vocal fold tissue has been developed. It does not include a representation of aerodynamics and therefore can accommodate increased detail in the vocal fold tissue representation. These models are valid when air pressure in the larynx is low, i.e. during closing and collision of the vocal folds during voice production. Three dimensional models with a spatial resolution of 250 μm, which is suitable for

examining stress distributions on the scale of pathology development, have been created using finite element techniques. One model uses a homogeneous material definition (Chapter 2,3), and another uses four distinct material definitions to represent the tissue layers that compose the vocal fold (Chapter 4). These models' predictions of collision force magnitudes are comparable to those measured in vitro in canine larynges and during in vivo human voice production (Chapter 5) and their deformations are consistent with qualitative clinical observations. A lumped mass model that is computationally efficient and has physiologically meaningful inputs, but has low spatial resolution has also been developed (Chapter 3). Its predictions of collision force magnitudes are comparable to those predicted by the three dimensional models.

These models rely on published data for geometric and material definition and on published collision force data for validation. There is a need for additional data that fully parameterizes vocal fold mechanics by representing behavior of the component materials in multiple deformation modes, directions and rates, and illustrating the deformation of the individual vocal fold layers. The former could be obtained using careful and creative studies of excised vocal fold tissue and would enhance the fidelity of the input parameters. The latter could be obtained using high spatial and temporal resolution imaging studies and would provide additional validation data. Comparisons with models that include aerodynamic representations would further test the model assumptions and improve accuracy of predictions.

Extensions of these models have the potential to be clinically useful surgical planning tools. Such extensions might predict aerodynamic waveforms using the glottal deformation predictions, and then apply speech synthesis techniques to predict acoustic

waveforms. This would provide a quantitative connection between surgical anatomy and sound. If well implemented, then it could be used to compare proposed alternative approaches to voice surgery.

METHOD FOR IN VIVO STUDY OF VOCAL FOLD COLLISION

In vivo measurements of vocal fold mechanics are necessary to quantify the mechanical environment of the vocal fold, but are difficult to make due to the small size of the larynx, its precarious location within the airway and the delicacy of tissue movement during voice production. A novel method of measuring mechanical quantities during vocal fold collision has been developed that does not interrupt the process of interest (i.e. voice production) (Chapter 5). It involves stabilizing thin, flat sensors between the vocal folds. In individuals with one medialized, nonvibrating vocal fold the sensor is rested against the nonvibrating fold. Vibration of the remaining fold occurs with a smooth mucosal wave and voice quality is maintained in a reasonable range. In individuals with two vibrating vocal folds either the entire sensor is placed against one fold and used to stop its vibration, or the posterior aspect of the sensor is clamped between the arytenoid cartilages. Using the latter technique, both vocal folds vibrate well and voice quality remains good.

Design challenges during the development of a thin, flat force sensor included sealing the sensor from the in vivo environment, minimizing noise and calibrating voltage output with force input. Collision force magnitudes measured in humans are of the same order of magnitude as those measured using an in vitro canine preparation and demonstrate a similar relationship between voice intensity and force magnitude. The collision forces measured in a human with no history of laryngeal pathology or surgery are of the same

order of magnitude as those measured in subjects with one rigid, non-vibrating vocal fold. These results provide validation for all three preparations: in vitro canine hemilarynx, in vivo human with one rigid vocal fold, and in vivo human with two soft folds. The latter has the highest fidelity with normal voice production, but is the most technically difficult and experimentally restrictive. The other preparations offer reasonable alternatives for the experimental study of voice mechanics.

Other thin, flat sensors have the potential to provide additional information regarding the mechanics of vocal fold collision. For example, multiple force sensors on a single panel would provide spatial resolution to force measurements and an indication of contact area. This information could be used to interpret less invasive measurements of vocal fold mechanics such as those obtained using electroglottography.

SUPPORT FOR MECHANICAL INJURY OF VOCAL FOLD TISSUE HYPOTHESIS

The theoretical models of vocal fold collision described above were used to investigate the validity of the hypothesis that mechanical stresses induced by collision between the vocal folds are responsible for structural and functional changes in vocal fold tissue that manifest as vocal nodules (Chapter 3,4). The finite element model of vocal fold tissue revealed elevation of compressive stresses in all three coordinate directions, and vertical shear stress on the plane parallel to the plane of collision during collision (Chapter 3). These stress elevations were maximal in the midmembranous location where vocal nodules are often found and were correlated with increases in driving force, an indicator of volume, which is a known risk factor for vocal nodule development. Vocal nodule histology is consistent with injury by these types of stresses.

The lumped mass model of vocal fold collision revealed a dependence of compressive stress perpendicular to the plane of collision on volume, vocal fold tissue layer thicknesses and stiffnesses (Chapter 3). The latter two observations suggest an explanation for varying risk for vocal fold injury between individuals since they are dependent on vocal fold anatomy as determined by genetics and environment, and vocal fold configuration as determined by voice production strategies (for example, manipulation of stiffness and tension to control pitch). Systematic variation of material properties and geometry in the finite element model would produce predictions of the spatial variation of multiple stresses and provide a clearer assessment of risk factors than the lumped element model does, but would be computationally expensive.

The predictions of the finite element model of vocal fold collision that incorporates a layered structure explore the role played by the stiffness of the superficial lamina propria (SLP) in vocal fold injury (Chapter 4). Decreasing SLP stiffness decreased normal and shear stresses in the SLP and epithelium, as well as normal and shear strains in the epithelium and therefore reduces epithelial injury risk. However, decreasing SLP stiffness increased normal and shear strains in the SLP. The effects of stress and strain in tissues with different properties are not understood. Therefore it is not clear how SLP stiffness affects SLP injury risk.

Experimental support of the proposed tissue injury modes could be provided by vocal fold tissue culture studies. Such studies would help to interpret the magnitudes of the stress tensor components in terms of injury risk. They could also be used to investigate the roles of stress vs. strain in causing functional changes in SLP cell lines in extracellular matrices of varying composition.

MEASUREMENT AND INTERPRETATION OF VOCAL FOLD COLLISION FORCES

The novel method of measuring in vivo vocal fold collision quantities described above has been used to obtain in vivo estimates of vocal fold collision forces, which are loads that may contribute to vocal fold injury (Chapter 5). The finite element model of vocal fold tissue during collision guides the interpretation of the force data in terms of tissue stress levels (Chapter 2).

The magnitude of the experimentally measured collision forces in the two subjects with one rigid, nonvibrating vocal fold correlate better with voice intensity than frequency. The magnitude of the theoretically predicted contact forces correlates with theoretical predictions of normal stress perpendicular to the plane of collision, vertical shear stress on the plane parallel to the plan of collision and Von Mises stress. These stresses are therefore candidates for vocal fold tissue injury that is associated with high volumes. There is no clear case for the dependence of collision force and by extension mechanical stress and voice injury on voice pitch.

A systematic examination of collision forces for different laryngeal anatomies (i.e. child, male, female) using different modes of voice production (i.e. pressed, chest, breathy) would shed additional light on contributions to vocal fold collision forces and by extension injury risk. Collection of muscle activity, subglottal pressure and anatomical information during these experiments would help to tease out the risks associated with different pitch manipulation mechanisms.

FUTURE DIRECTIONS

The theoretical and experimental studies presented in this thesis explore vocal fold tissue mechanics during the closure and collision phase of voice production and provide insight into mechanical injury of vocal fold tissue. The logical extensions of this work are along the lines of continuing exploration of the role of mechanical stress in vocal fold injury and further development of the finite element models of vocal fold tissue mechanics. Further exploration of the contributions of geometric and material properties of tissue to mechanical stress levels, combined with experimental studies of vocal fold tissue response to stress will refine the impact stress hypothesis and have the potential to generate concrete recommendations for voice injury prevention. Further development of the theoretical models might include comparison with models with full aerodynamics or combination with speech synthesis algorithms. These extensions have the potential to generate robust tools that would be useful in future voice science investigations and clinical practice.

BIBLIOGRAPHY

Alipour, F., Berry, D. A. and Titze, I. R. (**2000**), "A finite-element model of vocal-fold vibration," Journal of the Acoustical Society of America. **108**, 3003-12.

Alipour, F., Montequin, D. and Tayama, N. (**2001**), "Aerodynamic profiles of a hemilarynx with a vocal tract," Annals of Otology, Rhinology & Laryngology. **110**, 550-5.

Alipour, F. and Scherer, R. C. (**2000**), "Dynamic glottal pressures in an excised hemilarynx model," Journal of Voice. **14**,

Alipour-Haghighi, F. and Titze, I. R. (**1991**), "Elastic models of vocal fold tissues," Journal of the Acoustical Society of America. **90**, 1326-31.

Berke, G. S. and Gerratt, B. R. (**1993**), "Laryngeal biomechanics: An overview of mucosal wave mechanics," Journal of Voice. **7**, 123-8.

Berry, D. A., MOntequin, D. W. and Tayama, N. (**2001a**), "High-speed digital imaging of the medial surface of the vocal folds," Journal of the Acoustical Society of America. **110**, 2539-47.

Berry, D. A. and Titze, I. R. (**1996**), "Normal modes in a continuum model of vocal fold tissues," Journal of the Acoustical Society of America. **100**, 3345-54.

Berry, D. A., Verdolini, K., Montequin, D. W., Hess, M. M., Chan, R. W. and Titze, I. R. (**2001b**), "A quantitative output-cost ratio in voice production," Journal of Speech, Language, & Hearing Research. **44**, 29-37.

Buckmire, R. A. and Rosen, C. A. (**2001**), "Vocal polyp and nodules," eMedicine Journal. **2**, 1-11.

Chan, R. and Titze, I. (**2000**), "Theoretical modeling of viscoelastic shear properties of human vocal fold mucosa: Theoretical characterization based on constitutive modeling," Journal of the Acoustical Society of America. **107**, 565-80.

Chan, R., W. and Titze, I. R. (**1999a**), "Viscoelastic shear properties of human vocal fold mucosa: Measurement methodology and empirical results," Journal of the Acoustical Society of America. **106**, 2008-21.

Chan, R. W. and Titze, I. R. (**1999b**), "Hyaluronic acid (with fibronectin) as a bioimplant for the vocal fold mucosa," Laryngoscope. **109**, 1142-9.

Chandrupatla, T. R. and Belegundu, A. D. (**1997**), *Introduction to finite elements in engineering*, *2 Ed.*(Prentice-Hall, New Jersey)

Cotron, R. and Casper, J. K. (**1996**), *Understanding voice problems: A physiological perspective for diagnosis and treatment*, *2 Ed.*(Williams & Wilkins; a Waverly Company, Baltimore) 418

de Vries, M. P., Schutte, H. K., Veldman, A. E. P. and Verkerke, G. J. (**2002**), "Glottal flow through a two-mass model: Comparison of navier-stokes solutions with simplified models," Journal of the Acoustical Society of America. **111**, 1847-53.

Dikkers, F. G. (**1994**), *Benign lesions of the vocal folds: Clinical and histopathological aspects*, *Ed.*(Drukkerij Van Denderen B.V., Groningen, Netherlands)

Gray, S. and Titze, I. (**1988**), "Histologic investigation of hyperphonated canine vocal cords," Annals of Otology, Rhinology & Laryngology. **97**, 381-8.

Gray, S. D., Titze, I. R., Alipour, F. and Hammond, T. H. (**2000**), "Biomechanical and histologic observations of vocal fold fibrous proteins," Annals of Otology, Rhinology & Laryngology. **109**, 77-85.

Gunter, H. E. (**2003a**), "A mechanical model of vocal fold collision with high spatial and temporal resolution," Journal of the Acoustical Society of America. **113**, 994-1000.

Gunter, H. E. (**2003b**), "Modeling mechanical stresses as a factor in the etiology of benign vocal fold lesions," submitted for review.

Hess, M. M., Verdolini, K., Bierhals, W., Mansmann, U. and Gross, M. (**1998**), "Endolaryngeal contact pressures," Journal of Voice. **12**, 50-67.

Hillman, R. E., Holmberg, E. B., Perkell, J. S., Walsh, M. and Vaughan, C. (**1989**), "Objective assessment of vocal hyperfunction: An experimental framework and initial results," Journal of Speech & Hearing Research. **32**, 373-92.

Hirano, M., Kiyokawa, K. and Kurita, S. (**1988**), "Laryngeal muscles and glottic shaping," in *Vocal physiology: Voice production mechanisms and functions*, edited by O. Fujimara (Raven Press Ltd., New York) 49-65

Hirano, M., Kurita, S. and Nakashima, T. (**1983**), "Growth, development and aging of human vocal folds," in *Vocal fold physiology: Contempory research and clinical issues*, edited by D. M. Bless and J. H. Abbs (College-Hill Press, San Diego) 22-43

Holmberg, E. B., Hillman, R. E. and Perkell, J. S. (**1988**), "Glottal air-flow and transglottal air-pressure measurements for male and female speakers in soft, normal and loud voice," Journal of the Acoustical Society of America. **84**, 511-29.

Ikeda, T., Matsuzaki, Y. and Aomatsu, T. (**2001**), "A numerical analysis of phonation using a two-dimensional flexible channel model of the vocal folds," Journal of Biomechanical Engineering. **123**, 571-9.

Ishizaka, K. and Flanagan, J. L. (**1972**), "Synthesis of voiced sounds from a two-mass model of the vocal cords," The Bell System Technical Journal. **51**, 1233-68.

Isshiki, N. (**1964**), "Regulatory mechanism of voice intensity variation," Journal of Speech, & Hearing Research. **7**, 17-29.

Jiang, J., Lin, E. and Hanson, D. G. (**2000**), "Voice disorders and phonosurgery i: Vocal fold physiology," otolaryngologic clinics of north america. **33**, 699-718.

Jiang, J. J., Diaz, C. E. and Hanson, D. G. (**1998**), "Finite element modeling of vocal fold vibration in normal phonation and hyperfunctional dysphonia: Implications for the pathogenesis of vocal nodules," Annals of Otology, Rhinology & Laryngology. **107**, 603-10.

Jiang, J. J., Shah, A. G., Hess, M. M., Verdolini, K., Banzali, F. M. J. and Hanson, D. G. (**2001a**), "Vocal fold impact stress analysis," Journal of Voice. **15**, 4-14.

Jiang, J. J. and Titze, I. R. (**1993**), "A methodological study of hemilaryngeal phonation," Laryngoscope. **103**, 872-82.

Jiang, J. J. and Titze, I. R. (**1994**), "Measurement of vocal fold intraglottal pressure and impact stress," Journal of Voice. **8**, 132-44.

Jiang, J. J., Zhang, Y. and Stern, J. (**2001b**), "Modeling chaotic vibrations in symmetric vocal folds," Journal of the Acoustical Society of America. **110**, 2120-8.

Kakita, Y., Hirano, M. and Ohmaru, K. (**1981**), "Physical properties of vocal tissue: Measurements on excised larynges," in *Vocal fold physiology*, edited by M. Hirano and K. Stevens (University of Tokyo Press, Tokyo) 377-98

Kaneko, T., Masuda, T., Shimada, A., Suzuki, H., Hayasaki, K. and Komatsu, K. (**1987**), "Resonance characteristics of the human vocal fold in vivo and in vitro by an impulse excitation," in *Laryngeal function in phonation and respiration*, edited by T. Baer, C. Sasaki and K. S. Harris (Little, Brown and Company (Inc.), Boston) 349-65

Lieberman, P. (**1968**), "Direct comparison of subglottal and esophageal pressure during speech," Journal of the Acoustical Society of America. **43**, 1157-64.

Min, Y. B., Titze, I. R. and Alipour-Haghighi, F. (**1995**), "Stress-strain response of the human vocal ligament," Annals of Otology, Rhinology & Laryngology. **104**, 563-9.

Mossallam, I., Kotby, M. N., Ghaly, A. F., Nassar, A. M. and Barakah, M. A. (**1986**), "Histopathological aspects of benign vocal fold lesions associated with dysphonia," in *Vocal fold histopathology; a symposium*, edited by J. A. Kirchner (College Hill Press, San Diego) 65-80

Pawluk, D., Son, J., Wellman, P., Peine, W. and Howe, R. (**1998**), "A distributed pressure sensor for biomechanical measurements.," Journal of Biomechanical Engineering. **120**, 302-5.

Pelorson, X., Hirschberg, A. and van Hassel, R. R., Wijnands, A.P.J. (**1994**), "Theoretical and experimental study of quasisteady-flow separation within the glottis during phonation. Application to a modified two-mass model," Journal of the Acoustical Society of America. **96**, 3416-31.

Ressler, B., Lee, R. T., Randell, S. H., Drazen, J. M. and Kamm, R. D. (**2000**), "Molecular responses of rat tracheal epithelial cells to transmembrane pressure," American Journal of Physiology Lung Cell and Molecular Physiology. **278**, L1264-72.

Shipp, T. and McGlone, R. E. (**1971**), "Laryngeal dynamics associated with voice frequency change," Journal of Speech & Hearing Research. **14**, 761-8.

Stevens, K. N. (**1998**), *Acoustic phonetics.*(The MIT Press, Cambridge)

Story, B. H. and Titze, I. R. (**1995**), "Voice simulation with a body-cover model of the vocal folds," Journal of the Acoustical Society of America. **97**, 1249-60.

Swartz, M. A., Tschumperlin, D. J., Kamm, R. D. and Drazen, J. M. (**2001**), "Mechanical stress is communicated between different cell types to elicit matrix remodeling," Proceedings of the National Academy of Sciences of the United States of America. **98**, 6180-5.

Titze, I. R. (**1973**), "The human vocal cords: A mathematical model. I," Phonetica. **28**, 129-70.

Titze, I. R. (**1974**), "The human vocal cords: A mathematical model. Ii," Phonetica. **29**, 1-21.

Titze, I. R. (**1994**), "Mechanical stress in phonation," Journal of Voice. **8**, 99-105.

Titze, I. R., Lemke, J. and Montequin, D. (**1997**), "Populations in the u.S. Workforce who rely on voice as a primary tool of trade: A preliminary report," Journal of Voice. **11**, 254-9.

Titze, I. R., Schmidt, S. S. and Titze, M. R. (**1995**), "Phonation threshold pressure in a physical model of the vocal fold mucosa," Journal of the Acoustical Society of America. **97**, 3080-4.

Titze, I. R. and Story, B. H. (**2002**), "Rules for controlling low-dimensional vocal fold models with muscle activation," Journal of the Acoustical Society of America. **112**, 1064-76.

Titze, I. R. and Strong, W. J. (**1975**), "Normal modes in vocal cord tissues," Journal of the Acoustical Society of America. **57**, 736-49.

Titze, I. R. and Talkin, D. T. (**1979**), "A theoretical study of the effects of various laryngeal configurations on the acoustics of phonation," Journal of the Acoustical Society of America. **66**, 60-74.

Waters, C. M., Glucksberg, M. R., Lautenschlager, E. P., Lee, C. W., Van Matre, R. M., Warp, R. J., Salva, U., Healy, K. E., Moran, B., Castner, D. G. and bearinger, J. P. (**2001**), "A system to impose prescribed homogeneous strains on cultured cells," Journal of Applied Physiology. **91**, 1600-10.

Wong, D., Ito, M. R., Cox, N. B. and Titze, I. R. (**1991**), "Observation of perturbations in a lumped-element model of the vocal folds with application to some pathological cases," Journal of the Acoustical Society of America. **89**, 383-94.

Yamana, T. and Kitajima, K. (**2000**), "Laryngeal closure pressure during phonation in humans," Journal of Voice. **14**, 1-7.

Zeitels, S. M. (**1998**), "Phonosurgery - past, present & future," Operative Techniques in Otolaryngology - Head and Neck Surgery. **9**, 179.

Zeitels, S. M., Hillman, R. E., Desloge, R., Mauri, M. and PB, D. (**2002**), "Phonomicrosurgery in singers and performing artists: Treatment outcomes, management theories, and future directions.," Annals of Otology, Rhinology, & Laryngology. **190**, 21-40.

Zemlin, W. R. (**1997**), *Speech and hearing science; anatomy & physiology*, *4 Ed.*(Allyn & Bacon, Massachusetts) 610